united nations
educational, scientific
and cultural
organization

international atomic
energy agency

the
**abdus salam**
international centre for theoretical physics

H4.SMR/1150 - 27

**Fifth Workshop on Non-Linear Dynamics
and Earthquake Prediction**

**4 - 22 October 1999**

# Are big earthquakes predictable?
## A problem of the geometry of faults

*L. Knopoff*

University of California, Los Angles
Institute of Geohysics and Planetary Physics
Los Angeles, U.S.A.

# Are big earthquakes predictable?

## A problem of the geometry of faults

Leon Knopoff
UCLA

1. Healing
2. Dynamical modeling of fractures in 1, 2, 3 - D
   a. Stability to parameters
3. Faulting on non-planar geometry
4. Granularity in fault zones
5. Long-range correlations and interval time fluctuations
   a. Fault Networks

# PHYSICS OF THE EARTHQUAKE SOURCE: SUMMARY

- Inhomogeneity of geometry is an important determinant of seismicity
- Relaxation of stress at barriers must be understood
- Models of seismicity appear to be unstable with regard to many important ingredients
  - We have to get the geometry and the physics correct
  - What is the level of sensitivity that is needed so that the systems stabilize?
- It is doubtful that seismic time series are stationary, because of space-time interactions
  - We must consider the entire network of faults and not merely one linear structure
  - It is doubtful that the strain rates on individual faults are constants over time
- Dynamics and Dissipation are important ingredients in modeling seismicity
- Interaction on multiple time scales
- Fluid migration in faults plays an important part in the evolution of seismicity
- It is premature to construct the definitive model of seismicity of Southern California. Models that claim to give the "solution" to problems of seismicity are too simplistic, unstable, and unreliable.

## Physics, Theoretical and Numerical Issues
still to be solved

- To characterize earthquake histories in a multidimensional space of space, time, slip, energy, etc.
  We have to understand lack of stationarity of earthquake time series, and how to characterize episodicity
- To relate the physics of long-term stress degradation at sites of geometrical nonplanarity, such as stepovers, triple junctions, etc., to the short-term processes of iterative fractures
- To describe the physics of fracture on the smallest scales of fault-filling gouge and of geometrical irregularities on a scale smaller than the sizes of slips in the smallest earthquakes we can model
- To understand slip weakening processes in the time-scale (i.e. slip velocity scale) where dynamics is important
- To understand the healing process
- To understand the migration of fluids before, during and after earthquakes
- To figure out how we can model the influence on seismicity due to faults that have not yet been identified

III/13

- Inadequate size of computers: What are the relations between the sizes and speeds of computers and the sizes of the systems that we want to model?

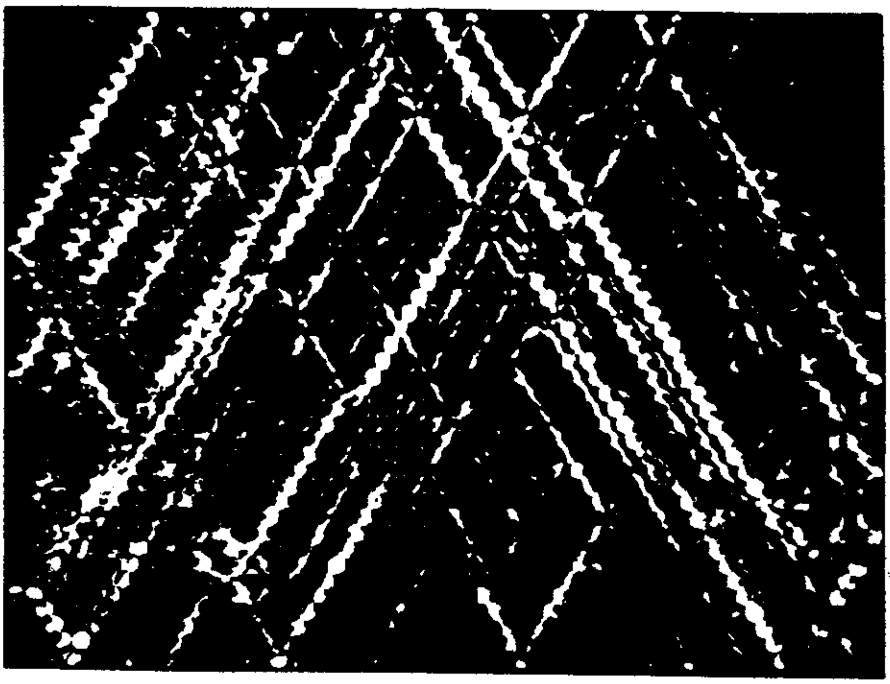

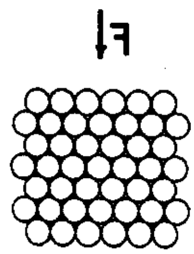


Fig. 4 — Photoelastic view of our 2d regular packing (triangular lattice). The horizontal arms are not much stressed.

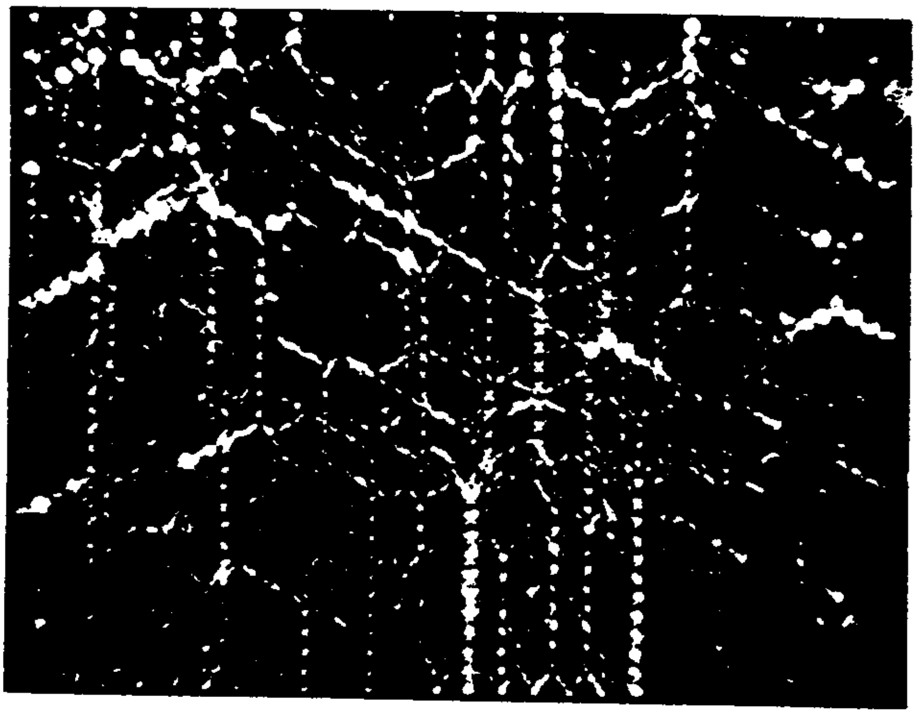

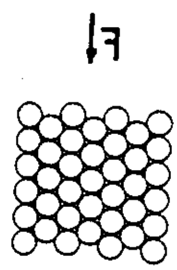


Fig. 5 — Photoelastic view of a packing similar to that on fig. 4 but turned by 30°. The transmission of the stresses through the vertical arms is important.

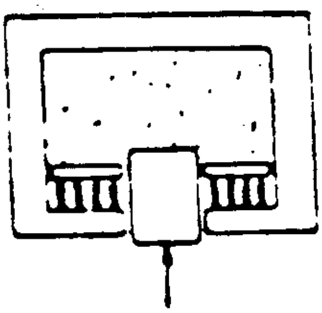

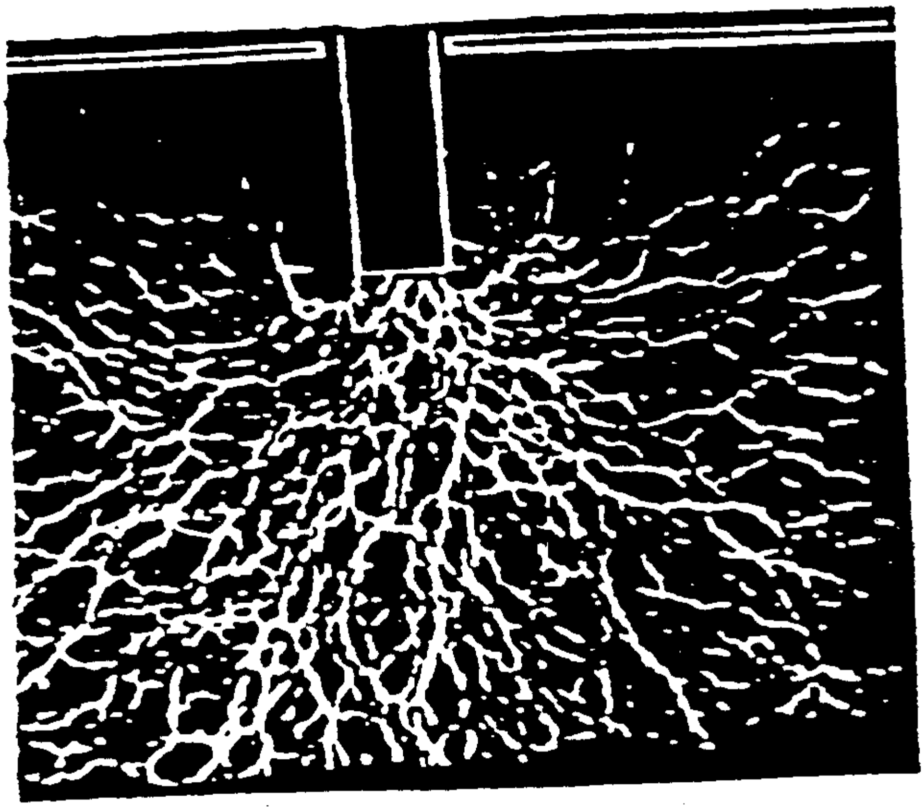

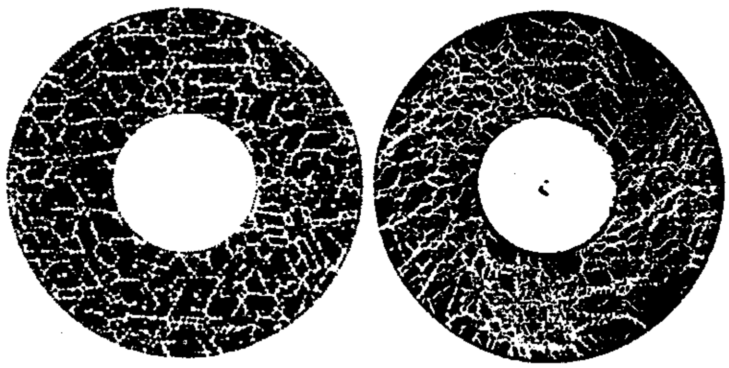

*Figure 4.* Pictures of the force-chains. (left) is an experiment showing the transparent light intensity. (right) is a simulation showing the potential energy stored in all contacts of one particle.

Figure 1:

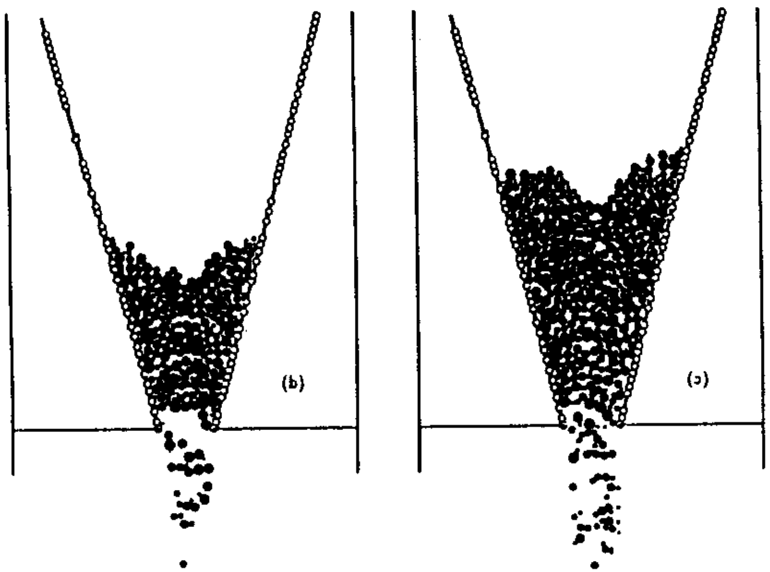


Figure 1:

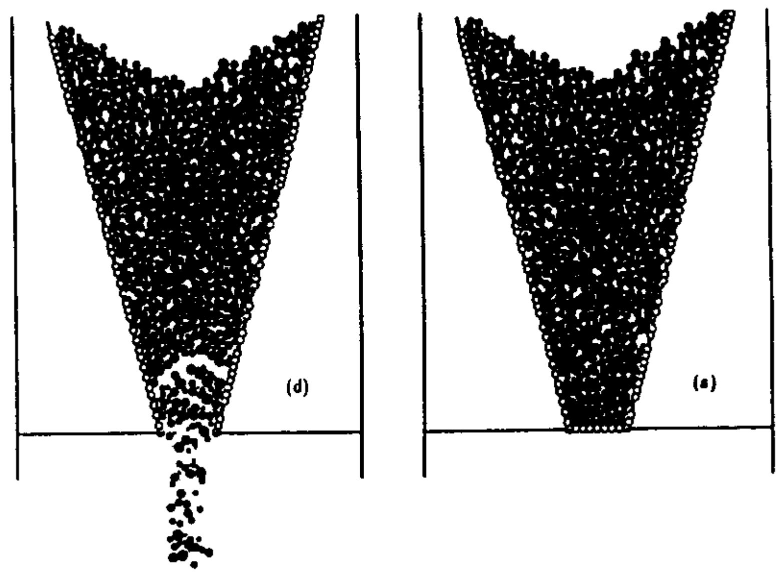

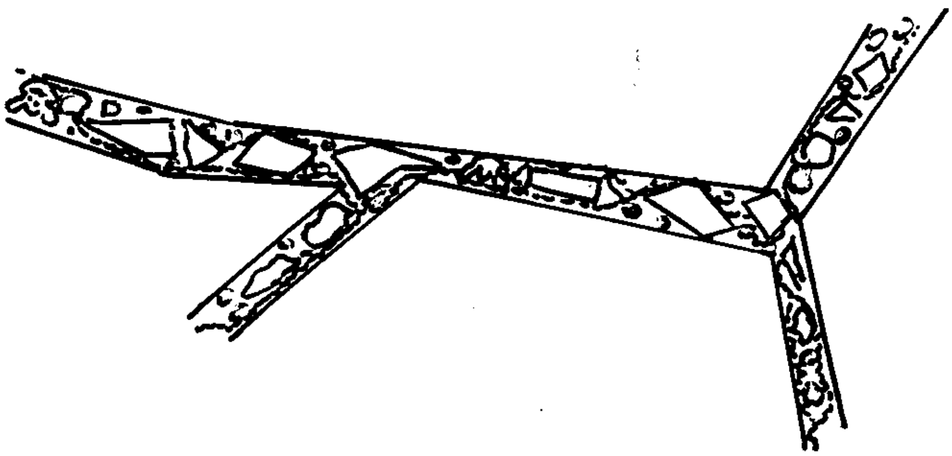

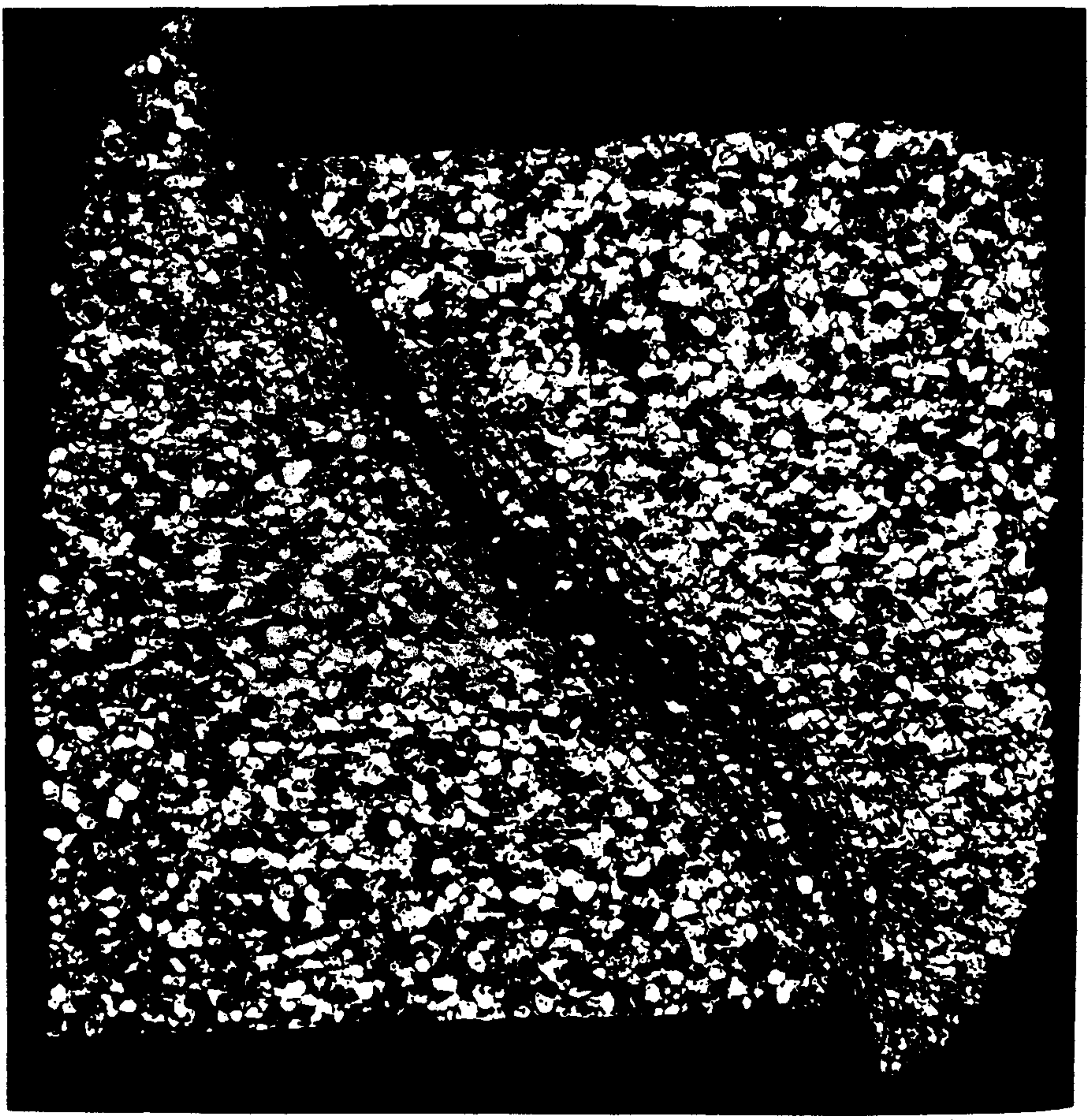

1 cm

ST. PETER SAND 48–65 MESH

Compacted at 500°C., 5 kb confining pressure, 1 kb interstitial water pressure, then compressed 40 per cent. perature and fluid pressures kept constant. Thick copper jacket did not rupture despite shear offset at ends.

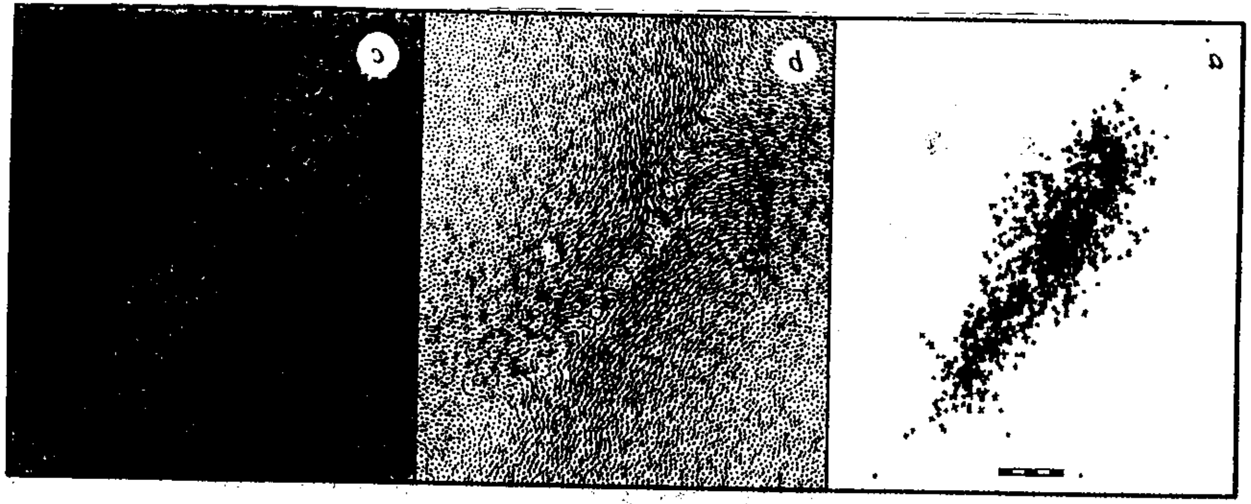


FIG. 3 'Coseismic' deformation for a time interval spanning the earthquake indicated in Fig. 2b; the behaviour shown is typical. The area shown is slightly smaller than the periodic cell. a, Locations of the acoustic emissions that define this earthquake. The size of each cross is proportional to the moment of the corresponding accoustic emission. b, Displacement vectors for each grain, defining a right-lateral strike-slip 'fault'. The displacements have been magnified by a factor of four, so the earthquake strain is approximately 1%. c, Volumetric strain derived from the displacement field; red and blue correspond to compaction and dilation respectively, with the most intense colours showing strains lying outside the limits of ±1%. The four prominent lobes correspond to the radiation pattern for compressional seismic waves from a strike-slip fault. In b, the two sides of the fault are separated by a zone of incoherent rotation and strain that is up to 5 grain diameters wide. This appears to be the sharpest dislocation that can be accommodated by the heterogeneous granular microstructure.

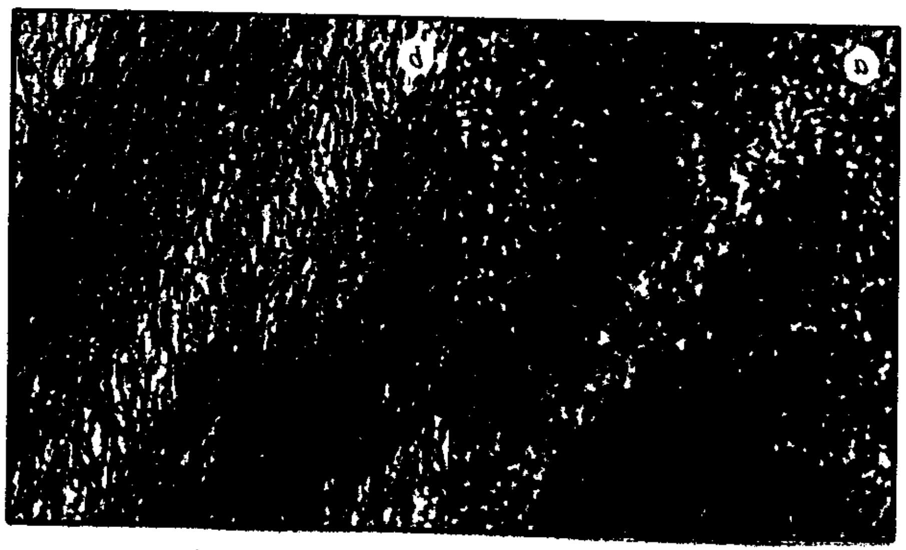


FIG. 4 Porosity and stress distributions immediately after the earthquake shown in Fig. 3; the patterns shown are typical. The area shown is slightly larger than the periodic cell. The porosity is shown in a; the lightest and darkest shades show porosities above and below the limits of 0.2 and 0.1 respectively. The stress distribution is shown in b. The colour of each grain ranges from yellow to red, indicating the ratio of shear stress to mean stress for that grain. Grains with relatively isotropic or hydrostatic loading are yellow, whereas those that are preferentially loaded in a single direction are red. In addition, the intensity of colour indicates the mean stress level, so that grains carrying relatively little load are pale. Lines of bright red grains show load-bearing bridges within the assemblage[36]. The compass points emphasize the local orientation of maximum compressive stress, averaged over a circular region of diameter equal to the length of the pointer. The main shear zone can be identified clearly in a and b. The porosity in the shear zone is greater than of the surroundings. The stress field outside the shear zone is relatively homogeneous and shows a uniform rotation of the maximum compressive shear zone is much more heterogeneous, with pale regions that carry very little load separated by red load-bearing bridges. The finite right-lateral strain of the shear zone has rotated these grain bridges, and hence the stress field, towards the perpendicular to the shear zone. The width of the

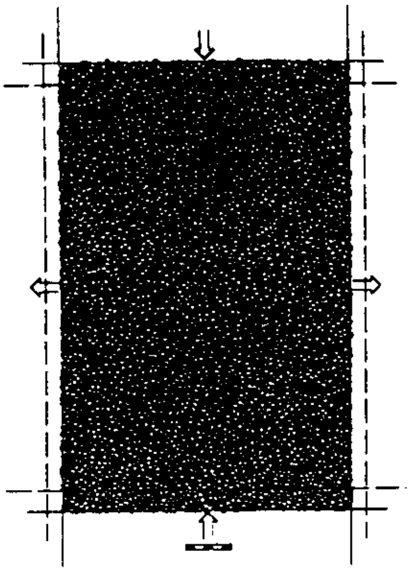

FIG. 1 The geometry used for the simulations is a two-dimensional rectangular cell that is periodic in both spatial dimensions. The cell contains an assemblage of $10^4$ circular grains of three sizes; the relative radii are 3:4:5, in proportions 5:3:2 respectively. This variation in radius prevents the grains from becoming ordered onto an hexagonal lattice; the assemblage is microscopically heterogeneous, and macroscopically both homogeneous and isotropic. To prepare the assemblage, non-overlapping grains are inserted at random into a cell of larger size and compacted by reducing the size of the cell. The shear test shown in Fig. 2 is conducted by shortening the periodic cell in one dimension and extending it in the other as indicated by the arrows; the assemblage is deformed in pure shear at constant volume. The shapes of the cell at the start and end of this deformation are shown by the solid and dashed outlines, respectively. The scale bars here and in Figs 3 and 4 have lengths of ~13 grain diameters.

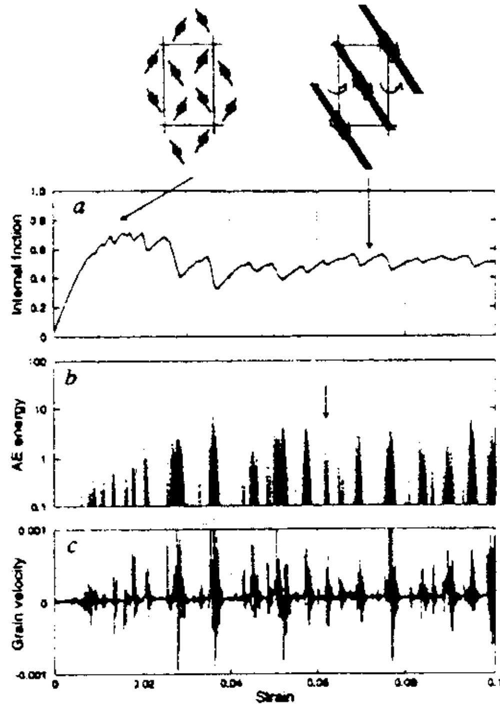


FIG. 2 Summary of results for shear deformation of the assemblage shown in Fig. 1. The horizontal axes shown strain, which is equivalent to time because the strain rate is constant. a, Internal friction, a measure of the ratio of shear stress to mean stress averaged over the assemblage. The sketches above the panel show the pattern of shear localization observed at two stages of the deformation (arrowed). b, Energy released by each acoustic emission (AE), scaled to the mean energy stored in a single elastic contact. The arrow indicates the earthquake illustrated by Fig. 3. c, One component of the velocity of a single grain within the sample, scaled to the speed of elastic waves in the granular assemblage. This 'seismogram' is smoothed over 100 time steps to show coherent, longer-period motions. Both the acoustic emissions and the seismogram show bursts of activity separating periods of quiescence.

are called 'acoustic emissions' (AEs), by analogy with laboratory tests on brittle materials in which acoustic energy is used to detect internal failure[11].

The main difficulty in DEM is efficient detection of new contacts that form during the arbitrary rearrangement of grains. In the code used here an adaptive graph[12] records and updates the local topology of grains and contacts. The equations of motion are solved using an explicit second-order finite-difference scheme, with a constant time step chosen to resolve accurately the motion of grains with the smallest natural period of vibration[9] (computed from the mass of a grain and the combined stiffness of its contacts). A small and uniform viscous damping force is applied to all grains, dissipating kinetic energy that would otherwise be trapped indefinitely by the periodic geometry. The resulting attenuation of elastic waves is independent of frequency[13], and the scale distance for dissipation of wave energy is chosen to match the size of the periodic cell.

Figure 2 shows both inelastic and elastodynamic information extracted from a typical simulation in which the ratio of mean stress to the elastic modulus of the grains in the compacted assemblage is approximately 0.01. This corresponds to a typical seismogenic depth of 10–20 km into the crust. The only other significant adjustable parameter is the loading speed, which is discussed below. The simulation reproduces the main features of mechanical tests on brittle materials. The initial deformation is uniform and elastic, but becomes inelastic as the energy and rate of AE increases. The stress climbs to a peak as the strain starts to localize onto a system of conjugate oblique shear zones, and then drops as the strain is localized to a single oblique shear zone. A persistent state is reached which, in this periodic geometry, corresponds to the shearing of an infinite deck of cards. The development of shear zones is a ubiquitous feature of deformation in soils[14] and rocks[15] and has been considered in numerical studies using granular[16,17] and continuum[18,19] mechanics, as well as in theoretical studies[20-22]. Two other features of the simulation invite comparison with geophysical observations.

First, the pattern of AEs mimics the basic characteristics of earthquakes. The AEs are clustered in time, each cluster representing an 'earthquake'. Figure 3 shows how the AEs in a single earthquake are localized in space and how the 'co-seismic' displacement and strain resembles that of a shear dislocation or strike-slip fault[23]. The long-term inelastic strain is produced by a series of such earthquakes within the shear zone. The rupture process is elastodynamic; once an earthquake has started it cannot be stopped by stopping the external loading, and its duration is determined by the elastic wave speed. The interval between earthquakes is, however, determined by the external loading speed. The ratio of loading speed to elastic wave speed in this simulation is approximately $10^{-5}$; the equivalent ratio for the deforming crust is around $10^{-12}$, so the intervals between real earthquakes are much longer relative to their duration. The loading speed in the simulation is, however, demonstrably slow enough to prevent earthquakes from blurring into one another (see Fig. 2b).

Second, although the shear zone is defined a locus of strain localization, it can also be identified in the stress field. Figure 4 shows that shear localization leads to dilation of the material within the shear zone and to a pronounced rotation of the orientation of maximum compressive stress. This rotation devel-

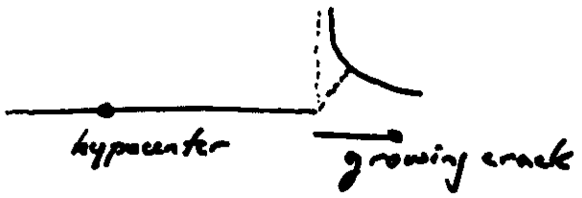


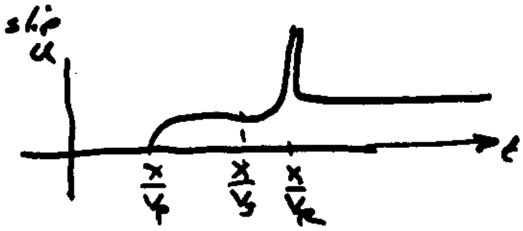


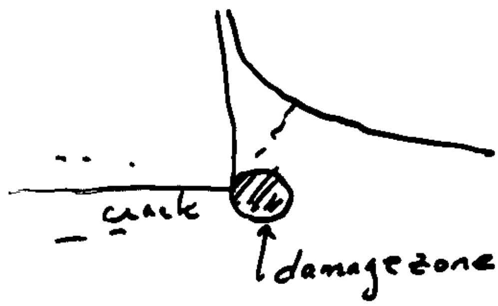


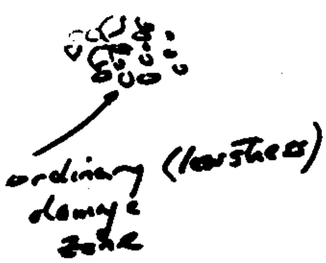


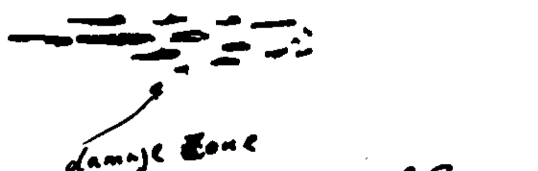


D. Scott Nature
Dec. 1996

SEISMIC REFLECTION DATA FOR THE SAN ANDREAS FAULT ZONE

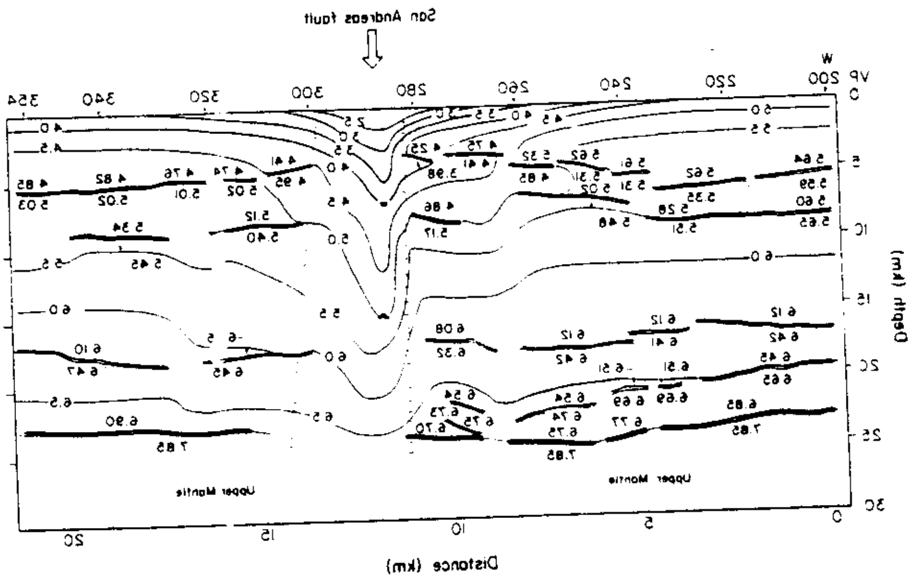

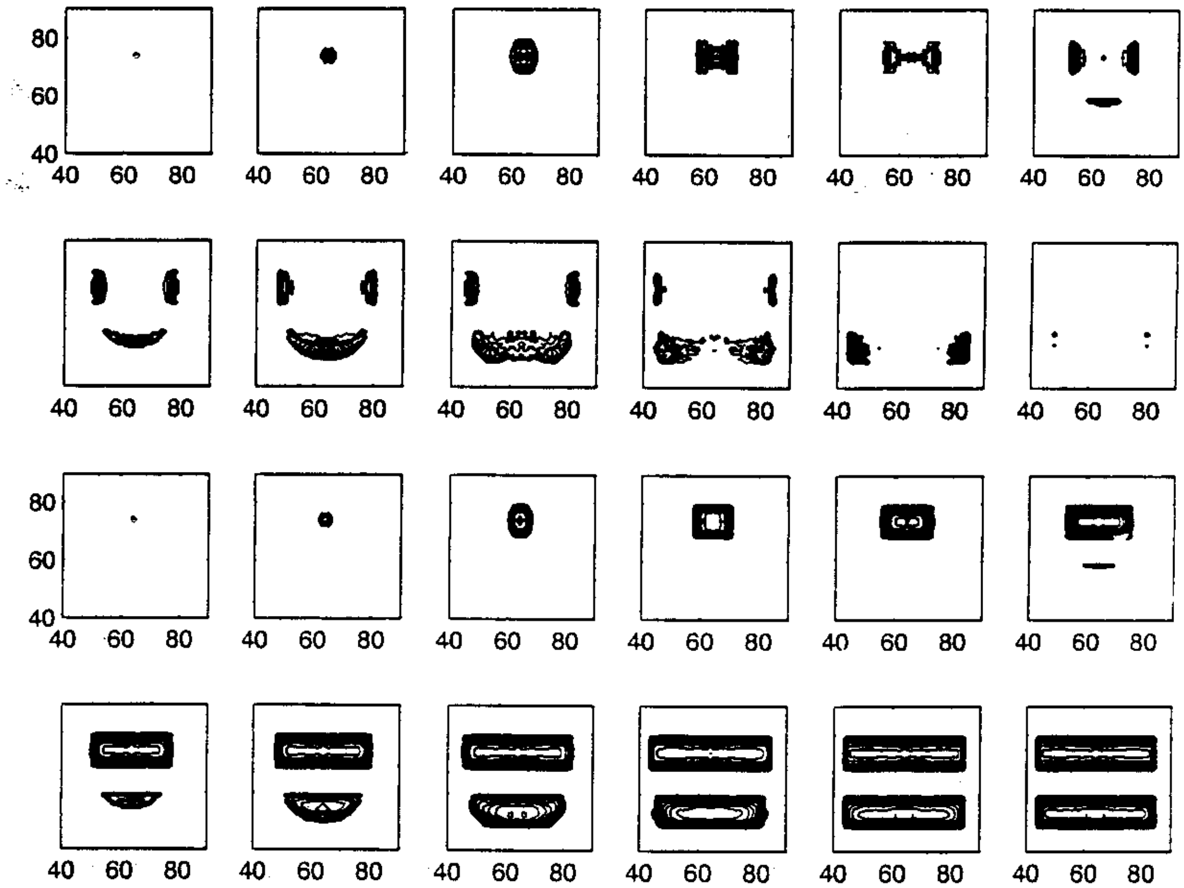
80
60
40
40 60 80

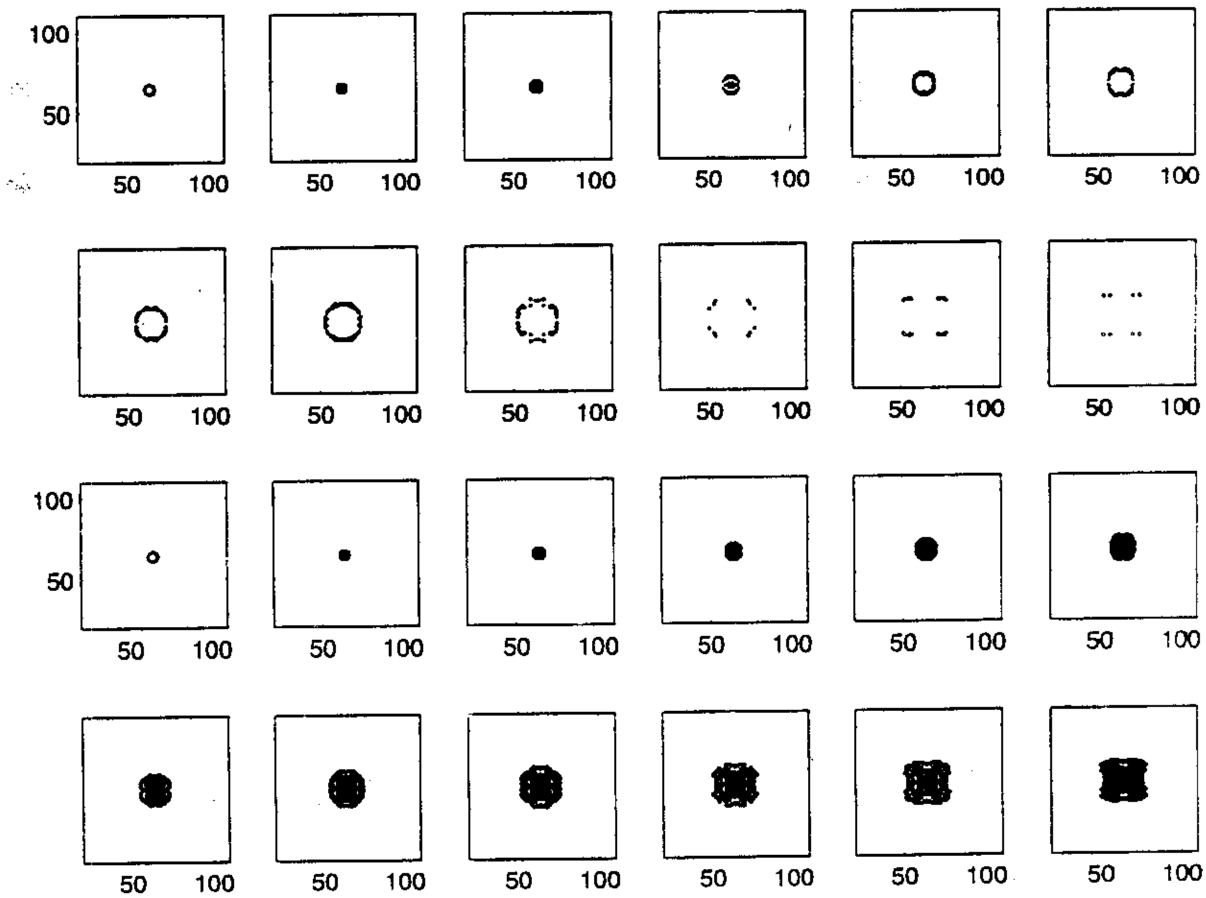
100
50
50
100

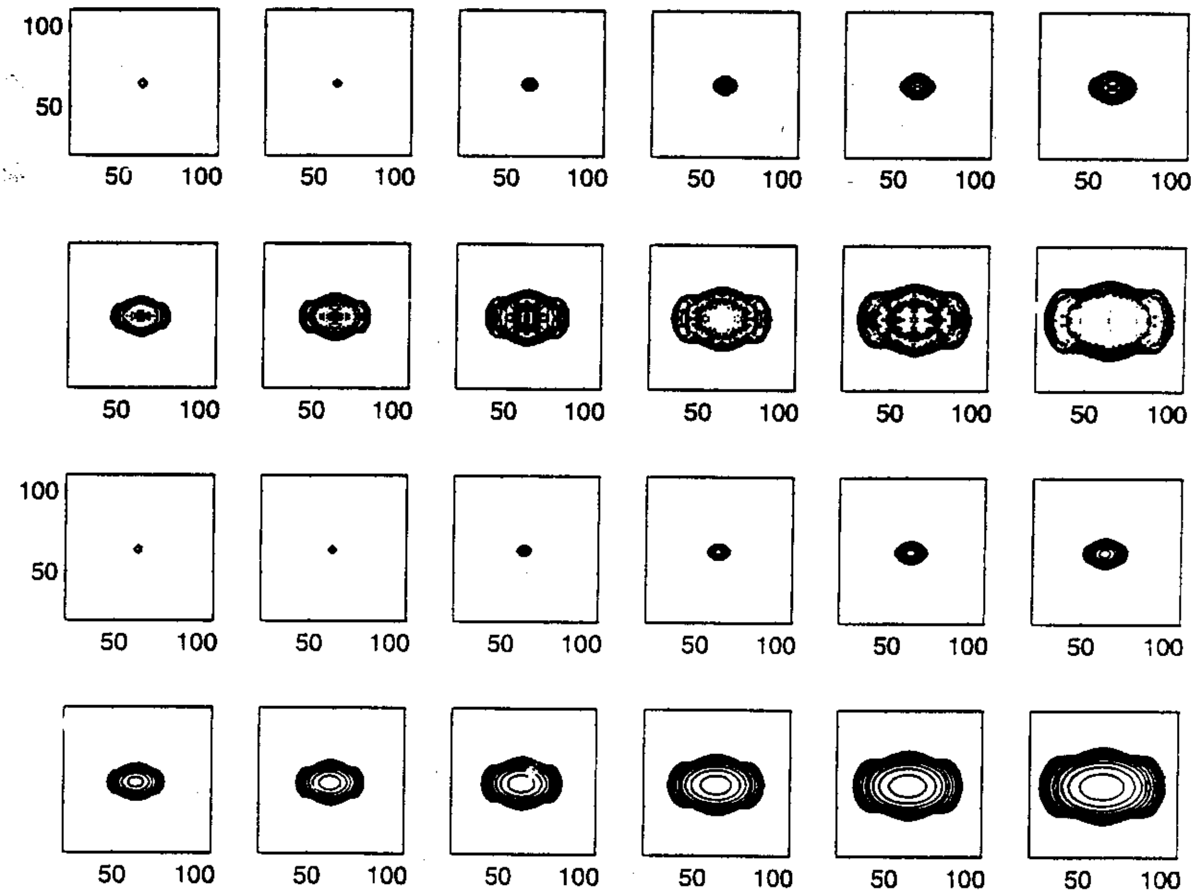
100
50
50
100

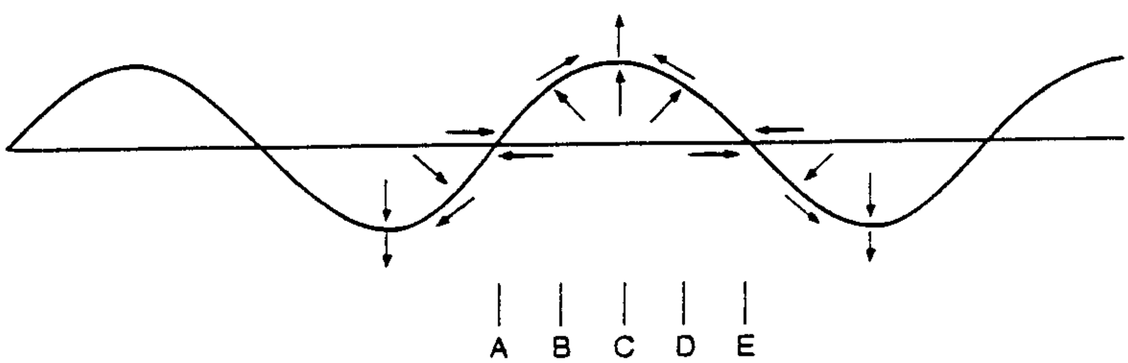


Fig. 4 Slip along a sinusoidal boundary moving to the right. The relative motions at selected points are indicated by the arrows. The motion at B is similar to that of Fig. 3.

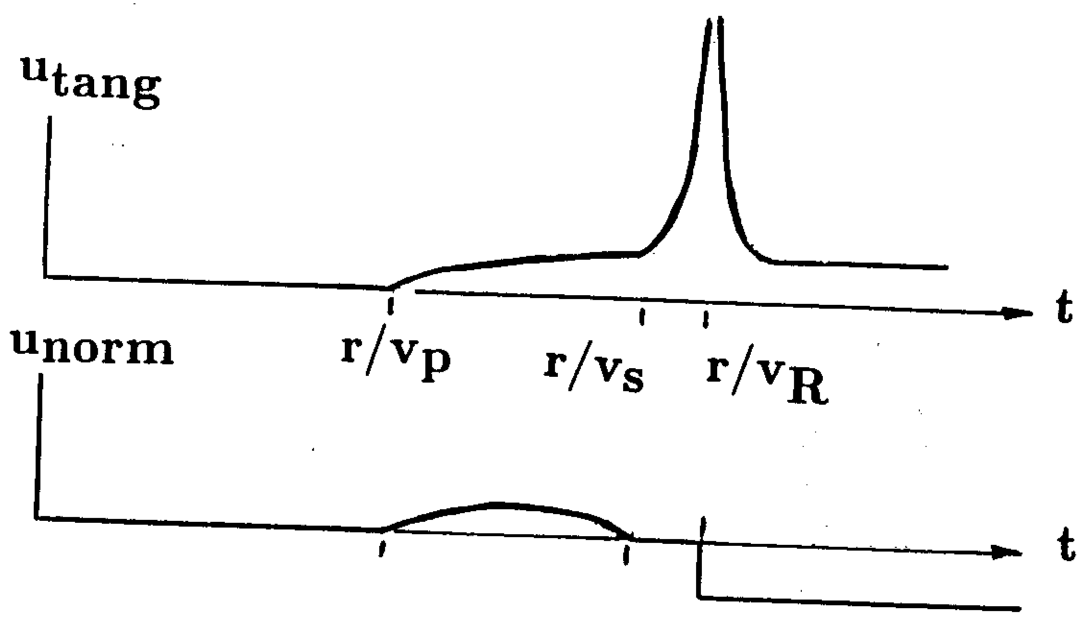

$u_{tang}$
$u_{norm}$
$r/v_p$
$r/v_s$
$r/v_R$
t
t

6.5

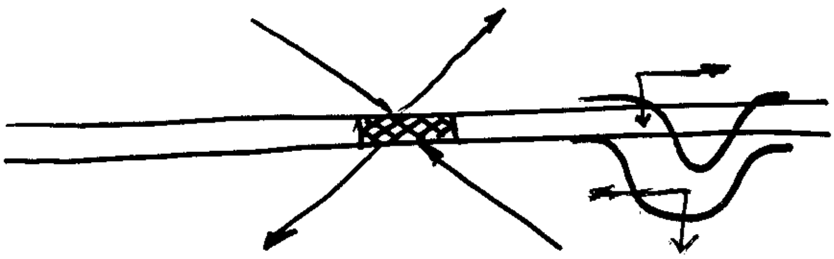

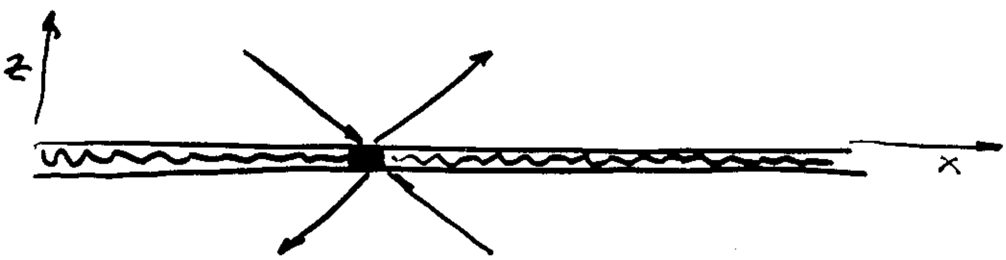


(or)  (or) $\tau_{xz}\; H(t-t_0)\,\delta(x-x_0)\,\Delta A$

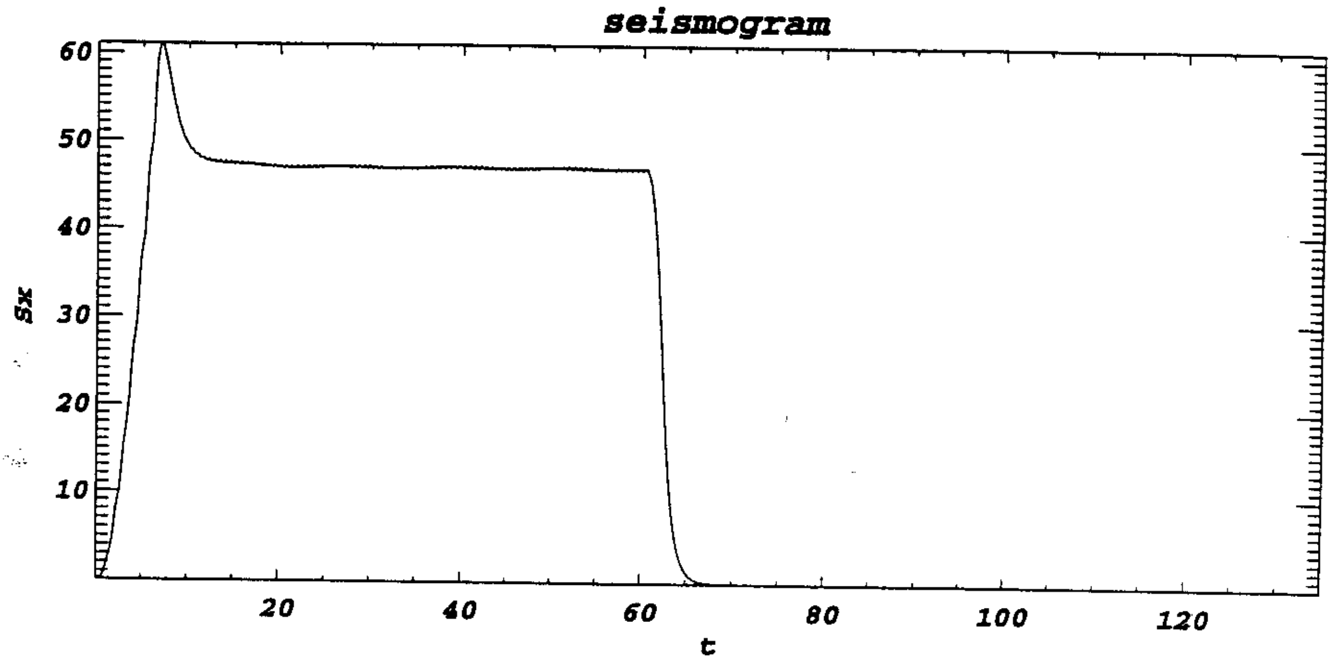
seismogram
Sx
t
60
50
40
30
20
10
20
40
60
80
100
120

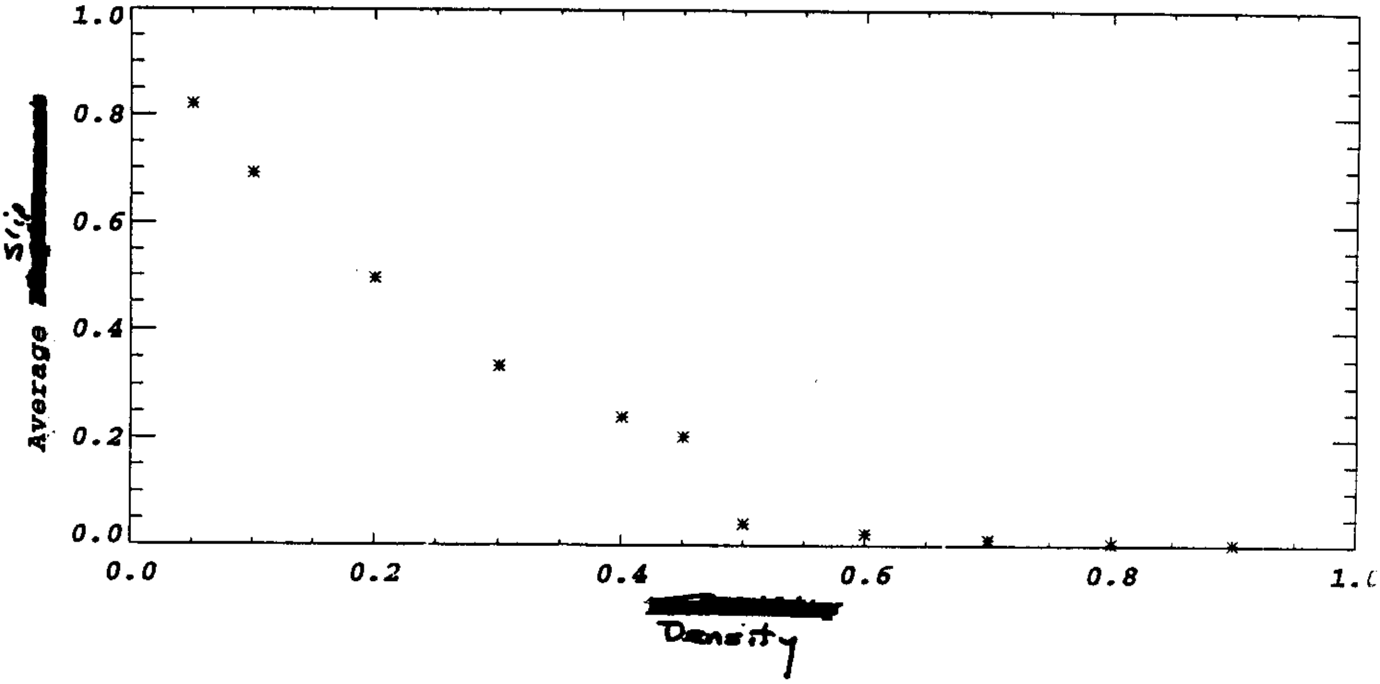
1.0
0.8
0.6
0.4
0.2
0.0
Average [redacted] Slip
0.0
0.2
0.4
0.6
0.8
1.0
[redacted] Density

l=0.

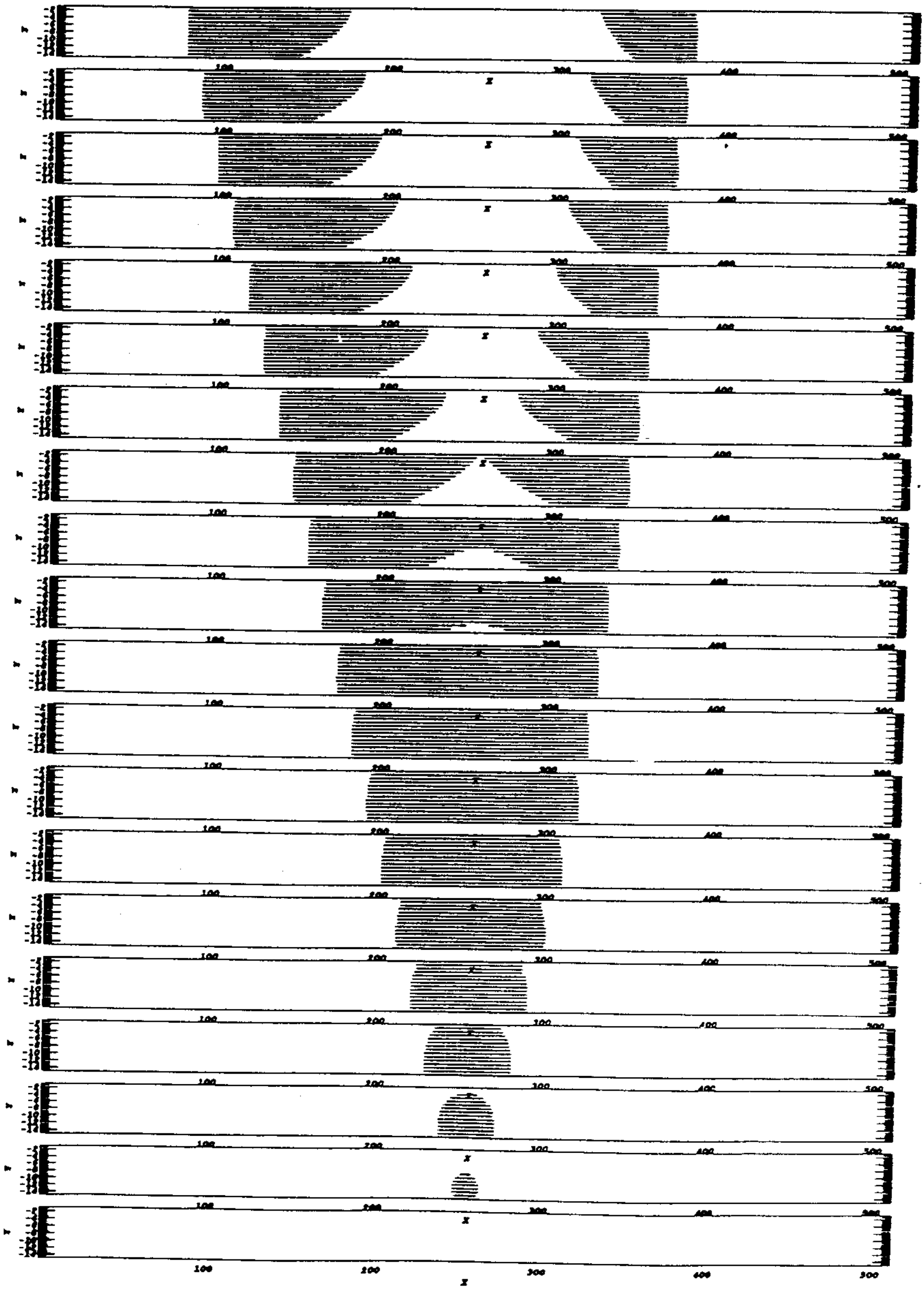


P0.1

$l = 1$

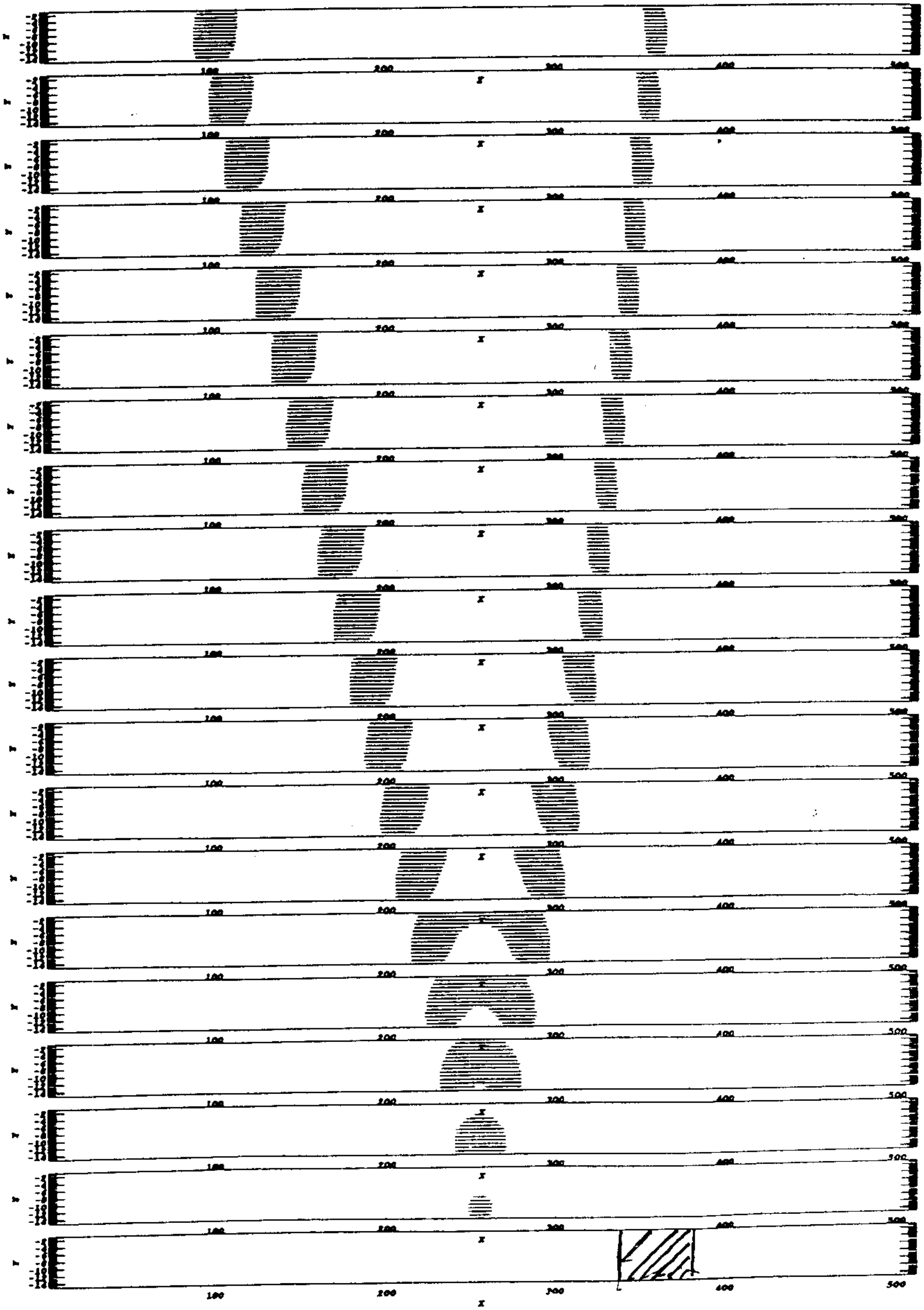

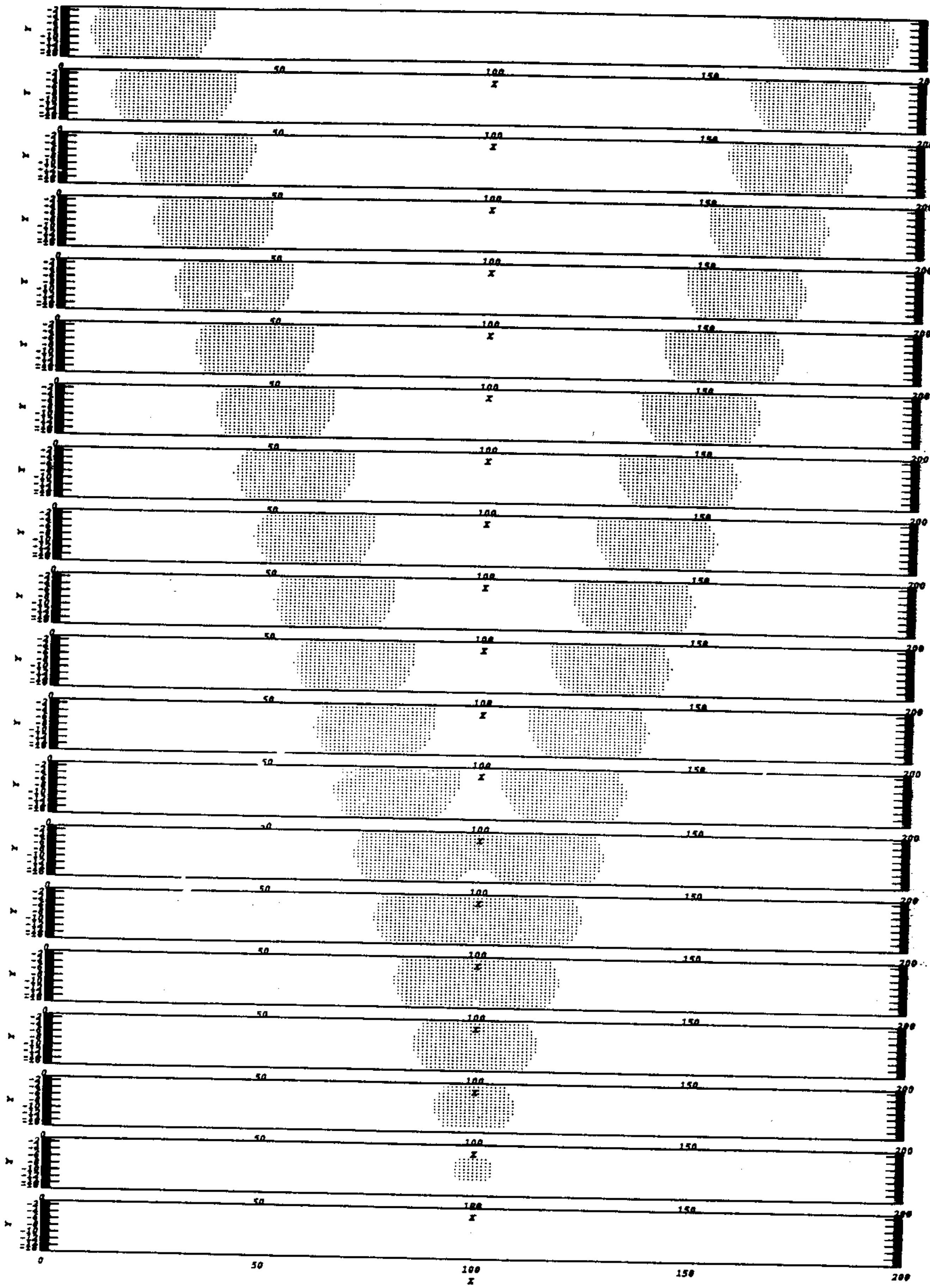


Ш3

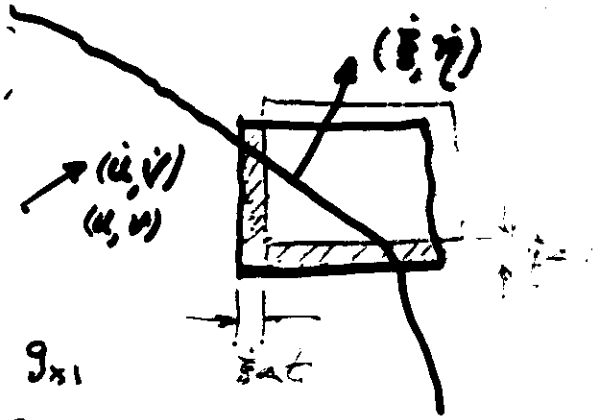


Momentum

$$-\rho u_t \dot{\xi} + (\lambda+2\mu)u_x + (\lambda+\mu)v_y = g_{x1}$$
$$-\rho u_t \dot{\eta} + \mu u_y + (\lambda+\mu)v_x = g_{x2}$$
$$-\rho v_t \dot{\eta} + (\lambda+2\mu)v_y + (\lambda+\mu)u_x = g_{y1}$$
$$-\rho v_t \dot{\xi} + \mu v_x + (\lambda+\mu)u_y = g_{y2}$$

---

Kinematic constraint

$$u_t + u_x\dot{\xi} + u_y\dot{\eta} = 0$$
$$v_t + v_x\dot{\xi} + v_y\dot{\eta} = 0$$

---

Fracture condition

$$G_x = g_{x1} + g_{x2} + T_x$$
$$G_y = g_{y1} + g_{y2} + T_y$$

Fracture if
$$\sqrt{G_x^2 + G_y^2} \geq B(x,y)$$

$\vec{T}$ = prestress

$B$ = breaking strength

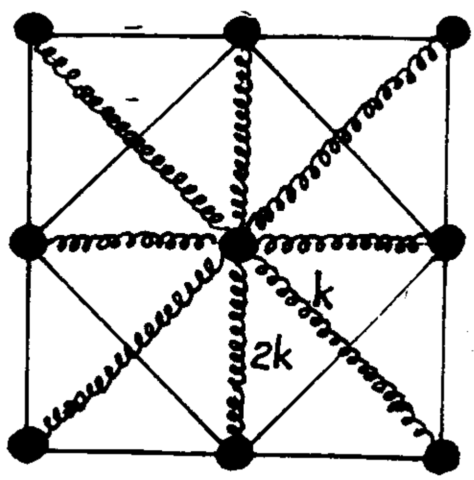


II
46
III
33

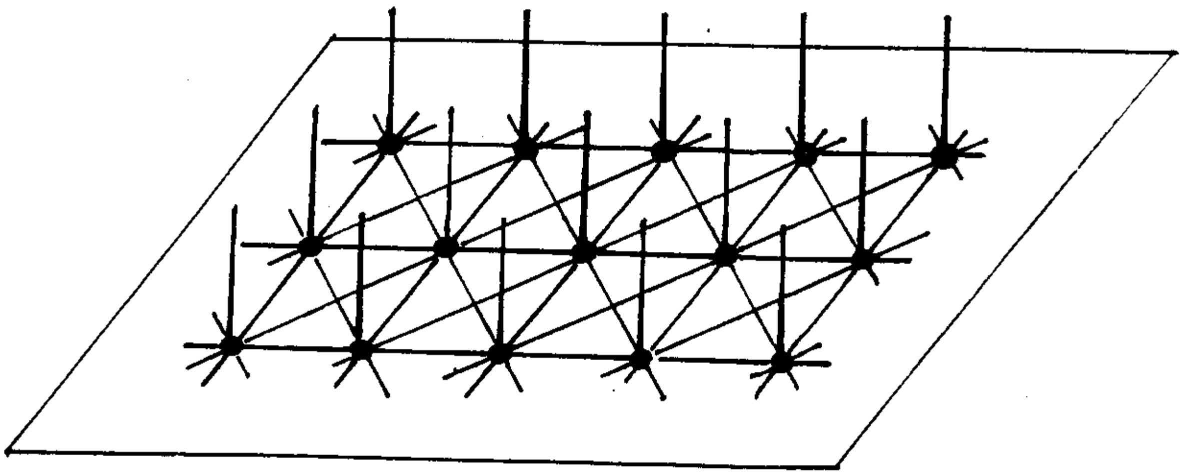

$$\rho \ddot{\vec{u}} = (\lambda+2\mu)\nabla\nabla\cdot\vec{u} - \mu\nabla\times\nabla\times\vec{u} - \ell(\vec{u} - V_0 t \hat{e}_x)$$
$$- \alpha\dot{\vec{u}} + \vec{T} - f_{frict}\frac{\dot{\vec{u}}}{|\dot{\vec{u}}|}$$

$$\alpha = 2\sqrt{\ell\rho}$$

$$\rho\ddot{u} = (\lambda+2\mu)\frac{\partial^2 u}{\partial x^2} + \mu\frac{\partial^2 u}{\partial y^2} + (\lambda+\mu)\frac{\partial^2 v}{\partial x\partial y} - \ell(u - V_0 t)$$
$$- \alpha\frac{\partial u}{\partial t} + T_x - f_f\frac{\dot{u}}{\sqrt{\dot{u}^2+\dot{v}^2}}$$

$$\rho\ddot{v} = (\lambda+2\mu)\frac{\partial^2 v}{\partial y^2} + \mu\frac{\partial^2 v}{\partial x^2} + (\lambda+\mu)\frac{\partial^2 u}{\partial x\partial y} - \ell v$$
$$- \alpha\frac{\partial v}{\partial t} + T_y - f_f\frac{\dot{v}}{\sqrt{\dot{u}^2+\dot{v}^2}}$$

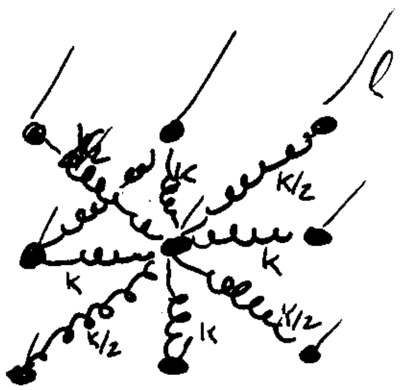


1820
Cauchy
Poisson
P. ratio = 1/4
$\underline{\lambda = \mu}$

II
45
J32

causality:

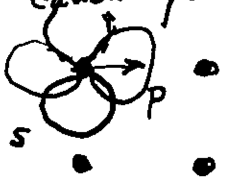

(scalar) elastic wave equation in 1-D

$$\mu \frac{\partial^2 u}{\partial x^2} = \rho \frac{\partial^2 u}{\partial t^2}$$

finite difference

$$\frac{m}{a}\ddot{u}_n$$

$$\mu\left[\frac{\left(\frac{u_{n+1}-u_n}{a}\right) - \left(\frac{u_n-u_{n-1}}{a}\right)}{a}\right]$$

$$= -k\left[2u_n - u_{n-1} - u_{n+1}\right]$$

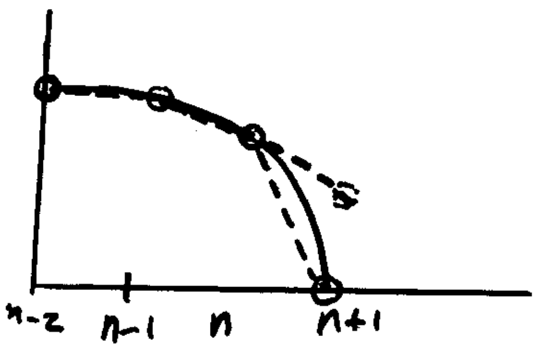


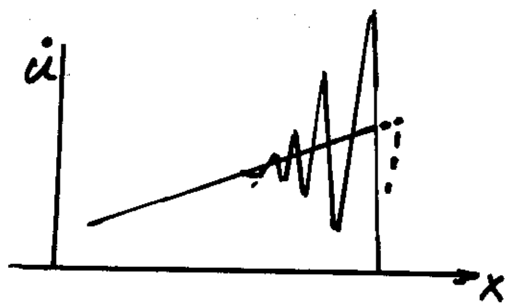

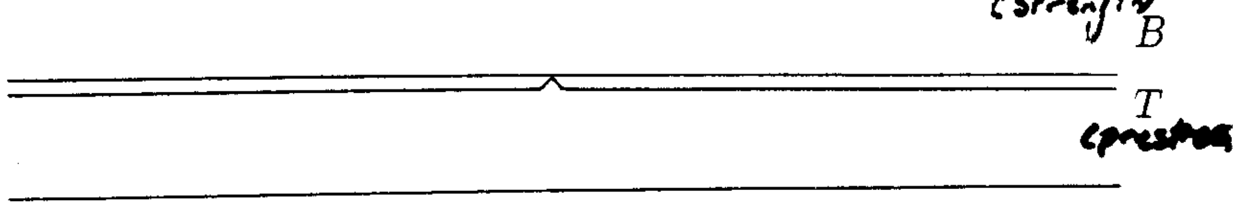


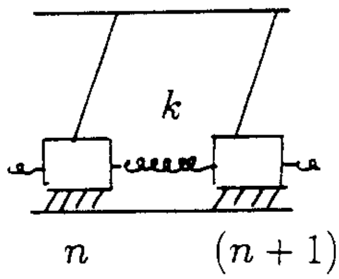


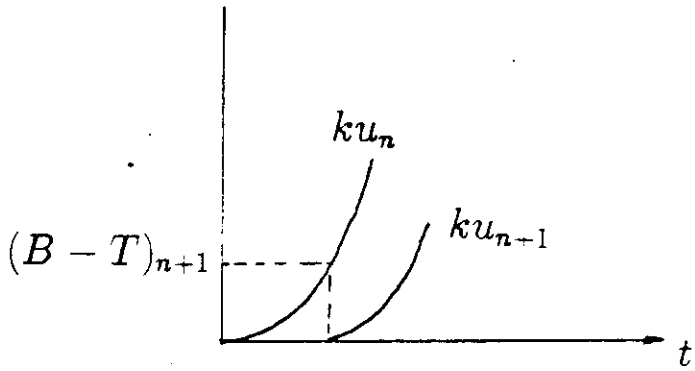


$$k(u_n - \cancel{u_{n+1}}) = (\text{Br. Str.} - T_{(pre)})_{n+1} = 0\ ?$$

$$k u_n \left(1 - \frac{a^2}{V_s^2 t^2}\right) = (B - T)_{n+1}$$

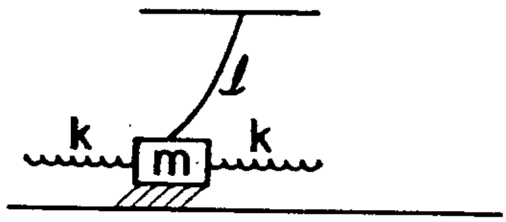


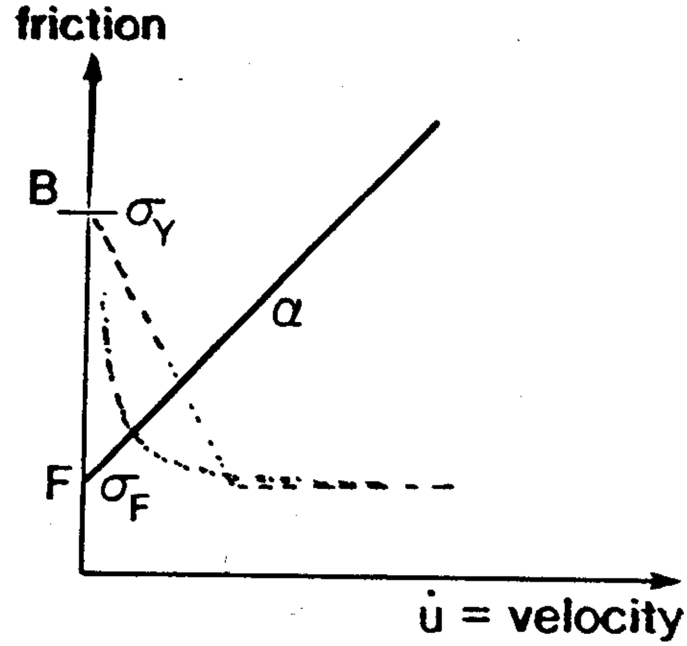


Dispersion

$$m\ddot{u} + k(2u_n - u_{n-1} - u_{n+1}) + \ell u_n = B_n - (F_n + \alpha \dot{u}_n)$$

$$\rho\frac{\partial^2 u}{\partial t^2} - \mu\frac{\partial^2 u}{\partial x^2} + \frac{\lambda u}{d^2} + \alpha\frac{\partial u}{\partial t} = (\sigma_Y - \sigma_F)$$

$$u = u_0 e^{i(kx-\omega t)}$$ Continuum Limit

$$\omega = -\frac{i\alpha}{2\rho} \pm \sqrt{\frac{\mu}{\rho}k^2 + \frac{\lambda}{\rho d^2} - \frac{\alpha^2}{4\rho^2}}$$

$$\text{if} \quad \alpha = \frac{2\sqrt{\lambda\rho}}{d}$$

$$u = u_0 \exp -\left(\frac{\alpha}{2\rho}t\right) \exp\left(i\omega\left(\frac{x}{c} - t\right)\right) \qquad c = \sqrt{\frac{\mu}{\rho}}$$

$\ell/k \Rightarrow$ Measure of dissipation

# Models
# DYNAMICS

Burridge-Knopoff (1967)

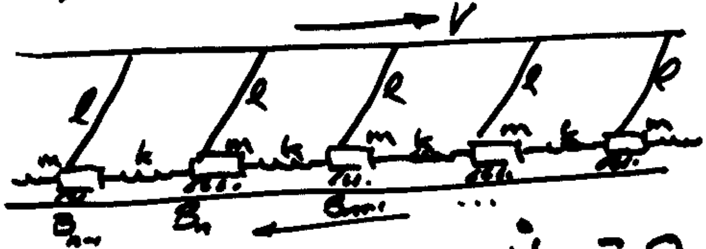


$$\rho\frac{\partial^2 u}{\partial t^2} - \mu\frac{\partial^2 u}{\partial x^2} + \lambda u$$

$$\dot{u}_n = 0$$

$$m\ddot{u}_n + k(2u_n - u_{n-1} - u_{n+1}) + \ell(u_n - Vt) = f_n$$

Defects: 1. No scaling in transverse direction

2. No elastic wave radiation to great distance

(1.) $\rho\frac{\partial^2 u}{\partial t^2} - \mu\frac{\partial^2 u}{\partial x^2} + \cancel{\lambda u} = \sigma(x)$ (Klein-Gordon eqn.)

(2)

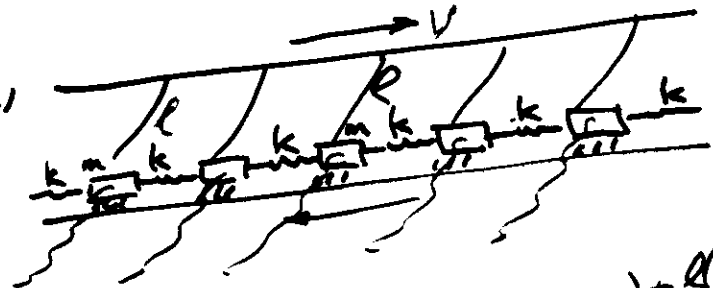


$$m\ddot{u}_n + k(2u_n - u_{n-1} - u_{n+1}) + \ell(u_n - \cancel{V}t) + \alpha\dot{u}_n = f_n$$

$e^{i(kx-\omega t)}$

Knop, Landoni, Abinani! Phys Rev 1992

3. Dispersion $\alpha = 2\sqrt{\ell m}$

4. Supersonic crack propagation

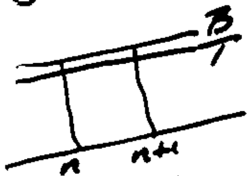


G.F.

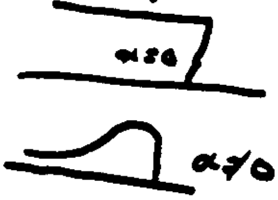


$$k(u_n - u_{n+1}) = B_{n+1} - T_{n+1}$$

$$k u_n\left(1 - \frac{a^2}{V_s^2 t^2}\right) = B_{n+1} - T_{n+1}$$

5. Shock-wave resonance

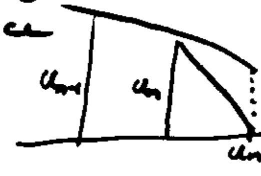


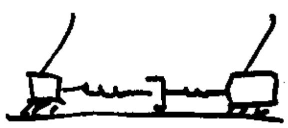

$$k \to k + \eta\frac{\partial}{\partial t}$$

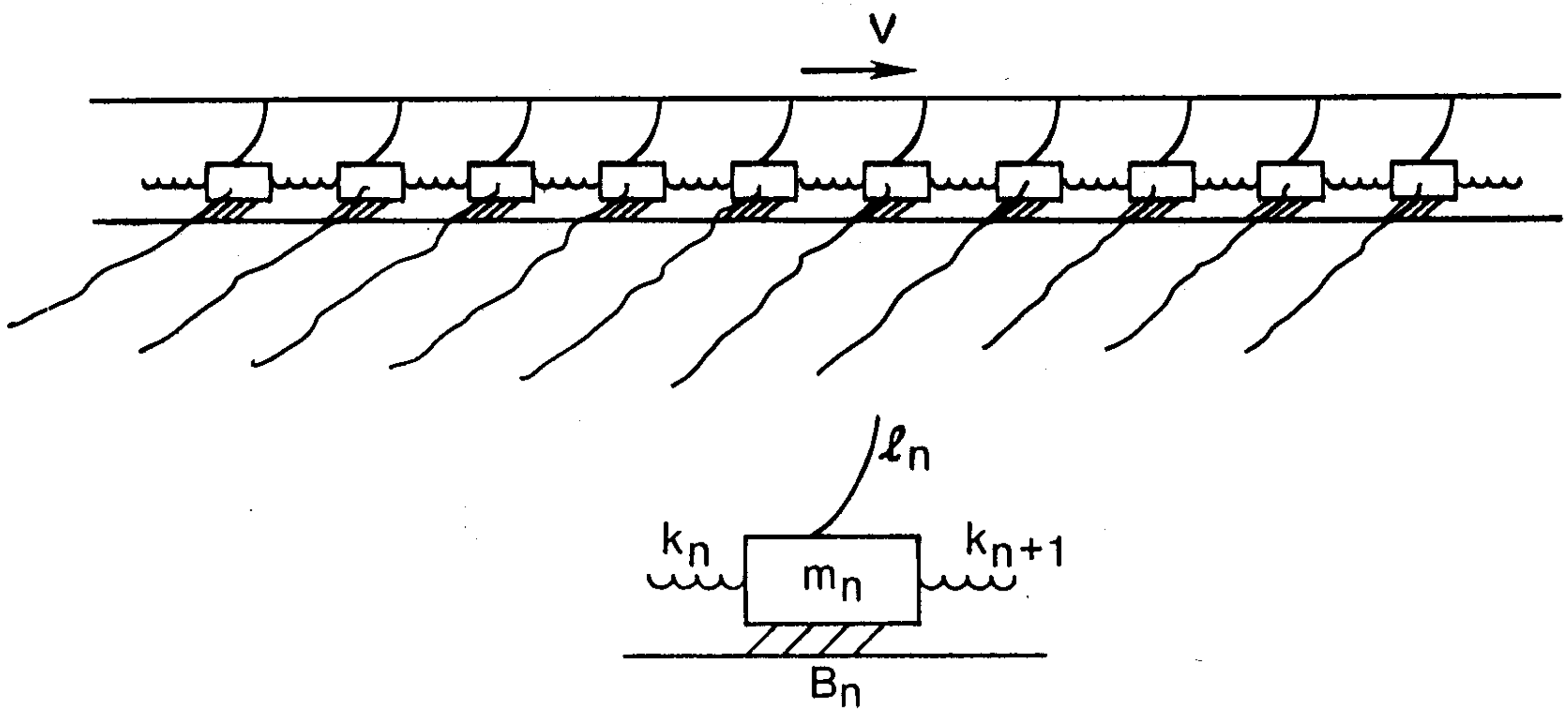


$$m\ddot{u}_n + k(2u_n - u_{n-1} - u_{n+1}) + \ell u_n + \alpha\dot{u}_n = f_n$$

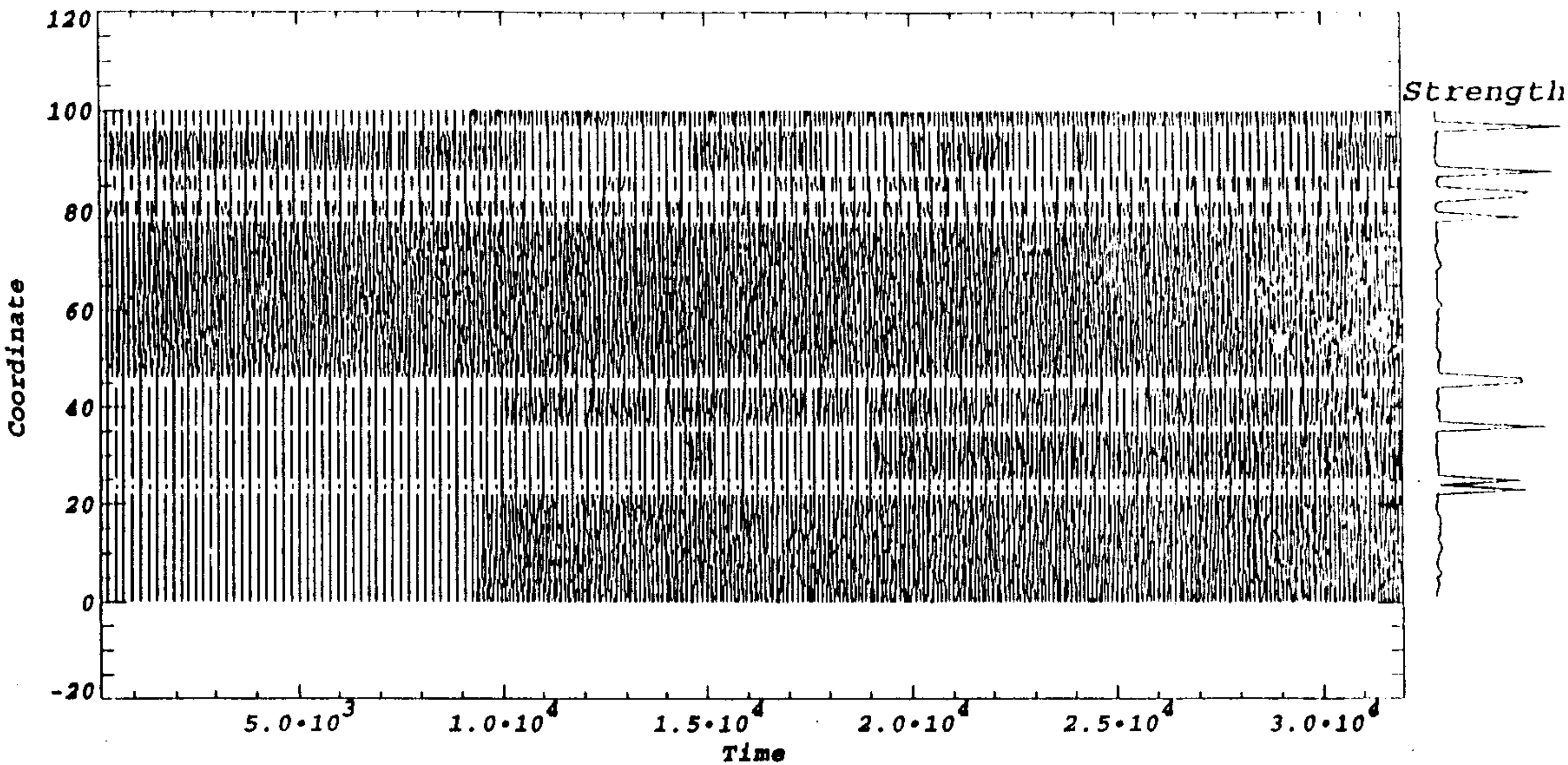
Coordinate
120
100
80
60
40
20
0
-20
5.0•10^3
1.0•10^4
1.5•10^4
2.0•10^4
2.5•10^4
3.0•10^4
Time
Strength

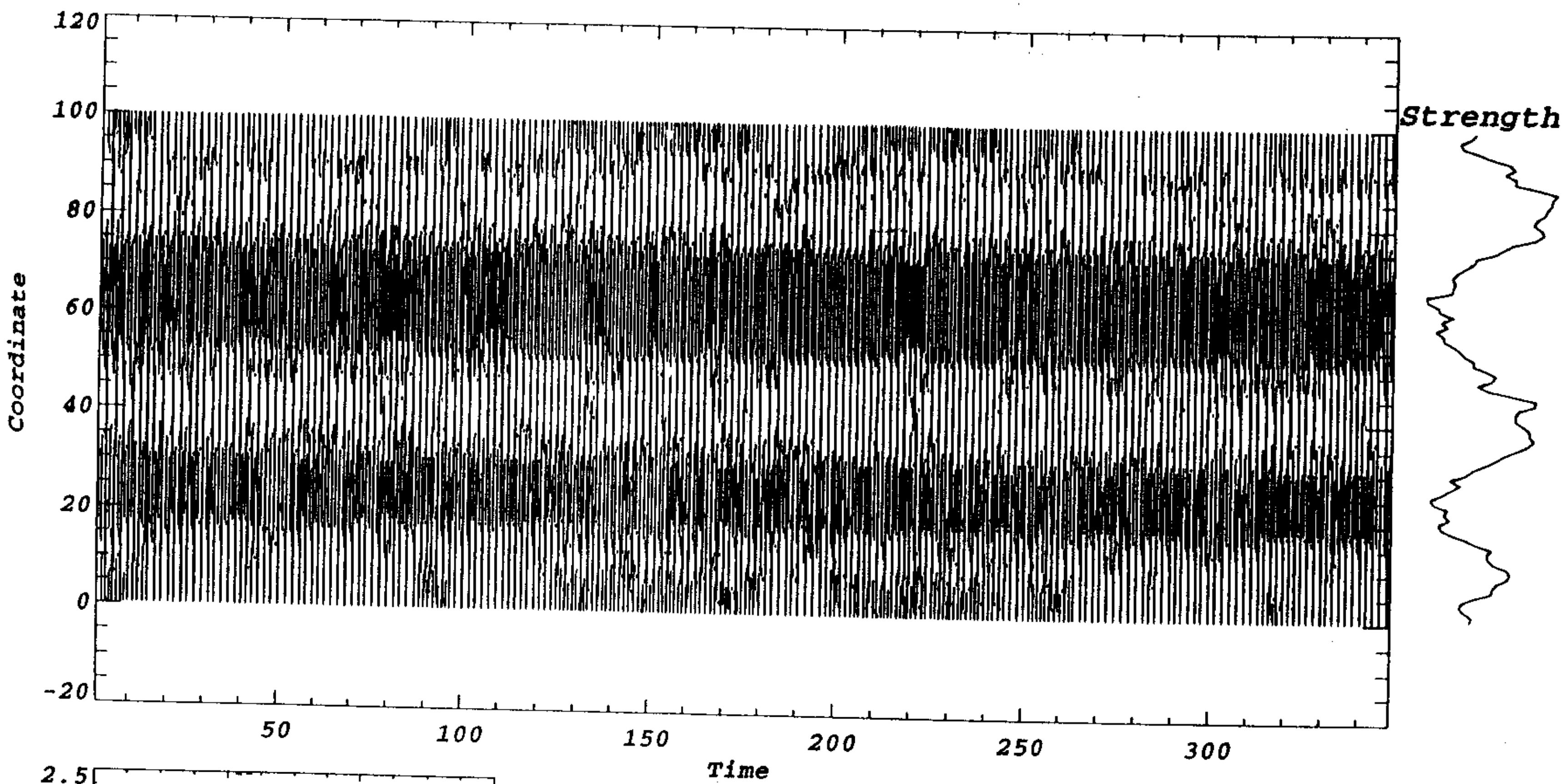


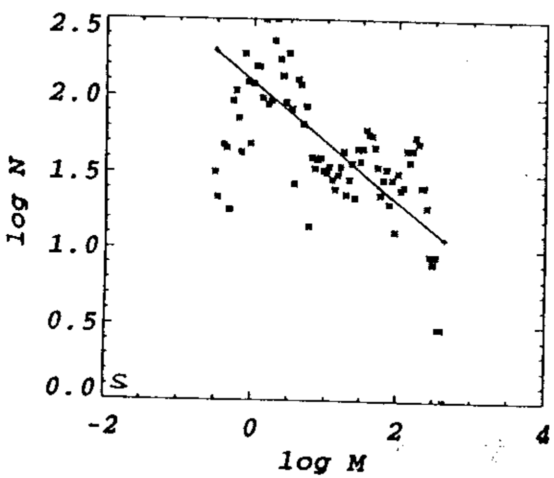


o/s = O

alpha=1.00, lfast=0.25
Bratio = 5.0, p=1.30
bmax=5.00 (#88), bmin=1.00 (#67)
bdyn=0.00, iseed=123457
5000 events, 100 masses
slope = -0.3876 1 s.d. = 0.041529

Masses in Motion vs Time

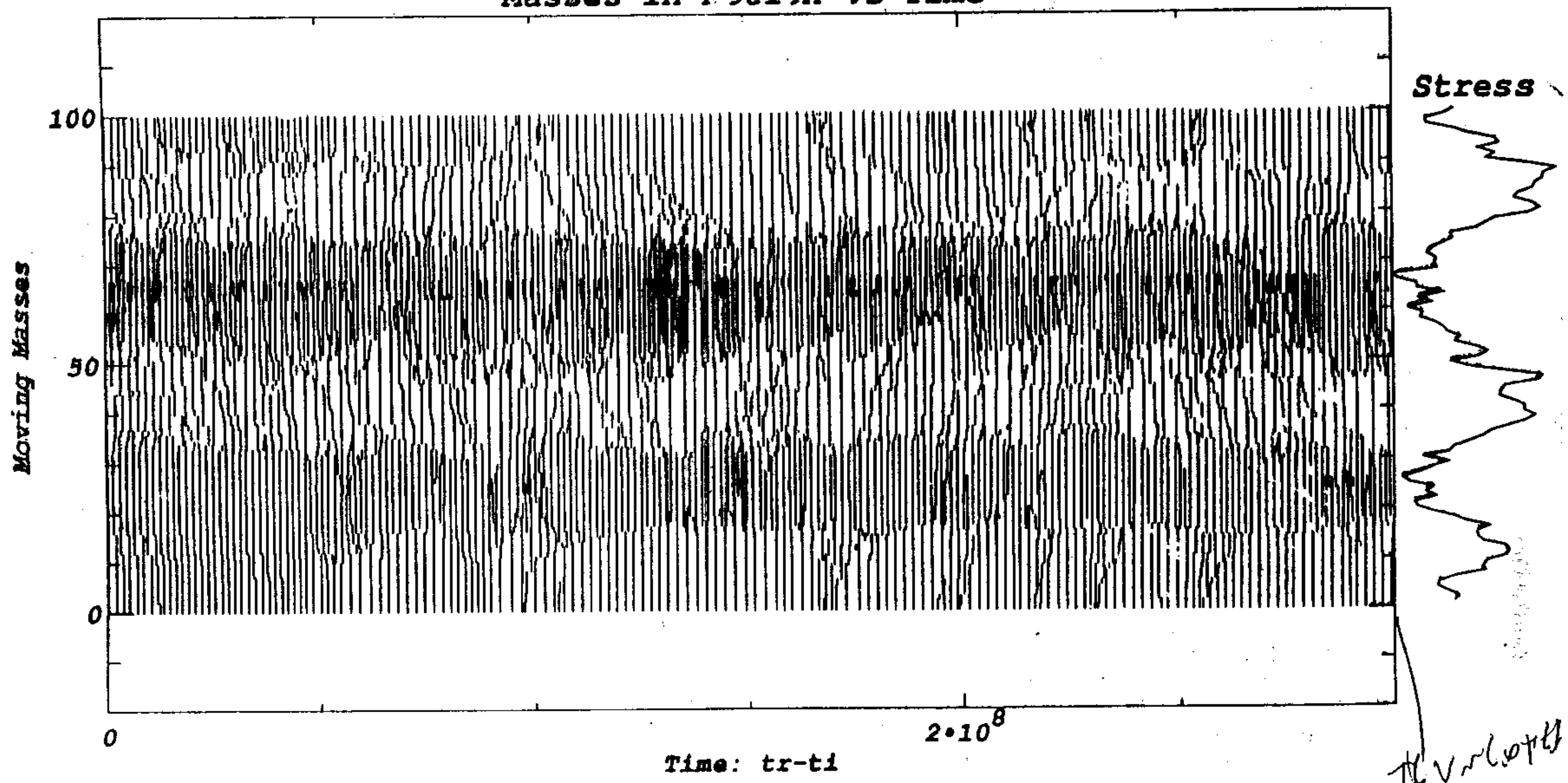


bmax=5.0 (#67), bmin=1.0 (#88), bdyn=0.0
r=0.5, alpha=1.0, v=1e-8
iseed=123457, p=1.5
5499 initial events
No discarded events
5499 analyzed events
tr=288.4e6 final time
ti=0.0 start time
( 6 digits trunk. in Stress )

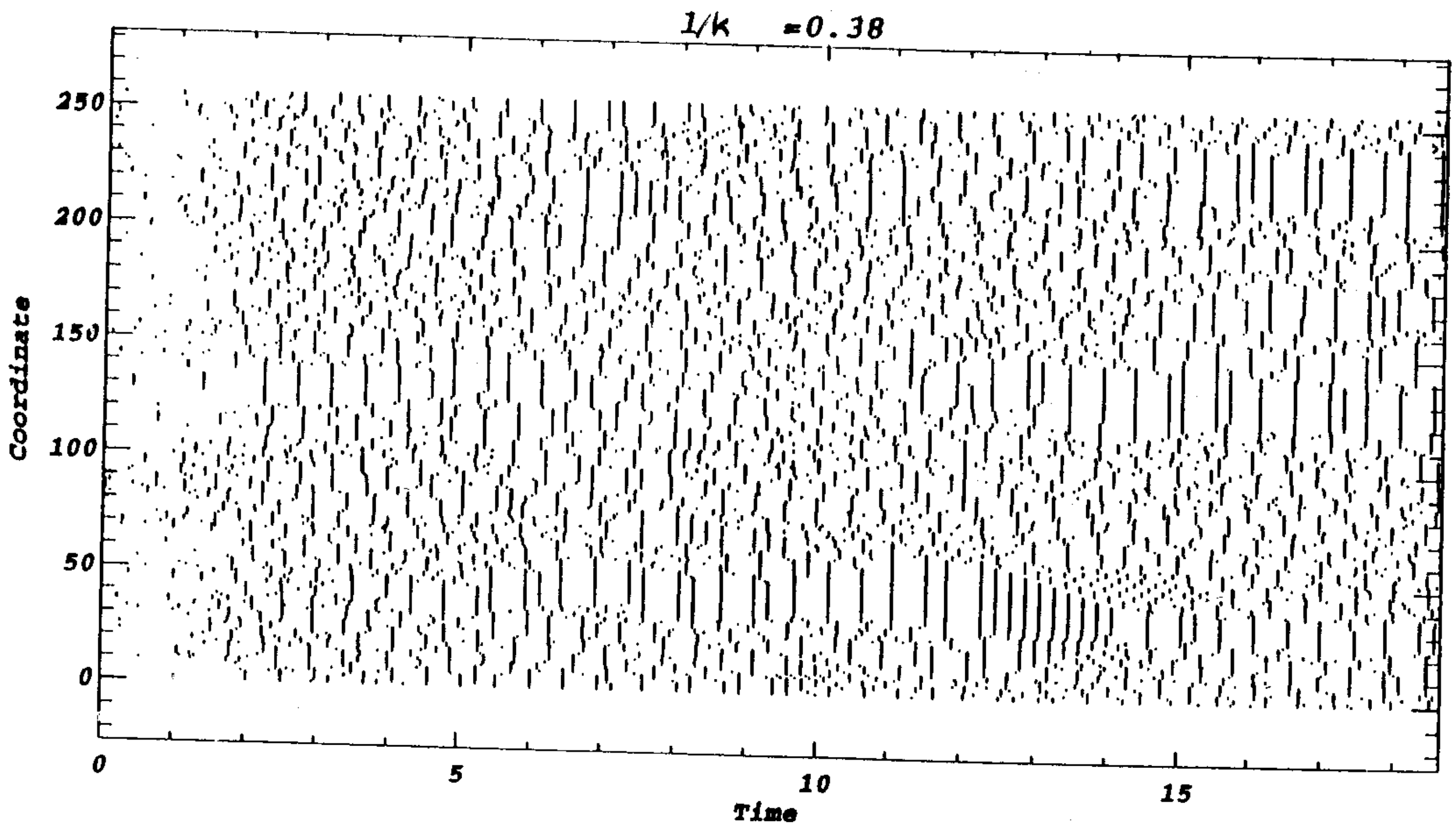
1/k =0.38
Coordinate
250
200
150
100
50
0
0
5
10
15
Time

est. $\gamma$: $\dfrac{\text{ht. of San Gabriel Mtns}}{\text{slip rate}} = \dfrac{3\text{ km}}{5\text{ cm/yr}} = 60{,}000\text{ yrs}$

shear strength

$$\sigma_t \to C_0\,(1 + \cancel{x}\,\gamma \sin 2\theta)$$

for $\gamma = 20$ ($\tau \sim 3000$ yrs)

$\dfrac{\sigma_t}{C_0} \to 30$

$\tilde{E}/E_{ss} \sim 900$

$\gamma = 400$

$\dfrac{\sigma_t}{C_0} \to 600$

$\dfrac{\tilde{E}}{E_{ss}} \sim 4\times10^5$

a mostly strike-slip fault with one compressional bend

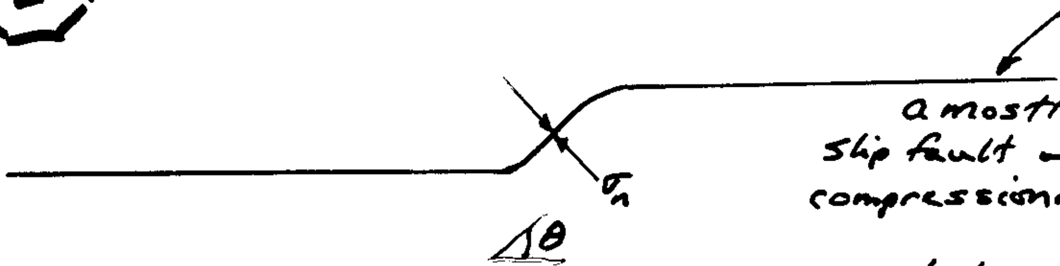


normal stress $\sigma_n$ is not relieved in bend eqs. so $\sigma_n$ increases with time

Either fault locks or stress $\sigma_n$ relaxes


I-9 CH3

$\gamma = \dfrac{\eta r}{C_0}$

1) (eqs.) brittle fracture in 3rd dim.
2) (viscous) creep
3) secondary faulting
   fault growth.

$C_0$ = shear strength

if $C_0 = \infty$, no relaxation $\Rightarrow$ locking $\Rightarrow$ plates stop

if $C_0 = 0$, all stresses relax $\Rightarrow$ no earthquakes

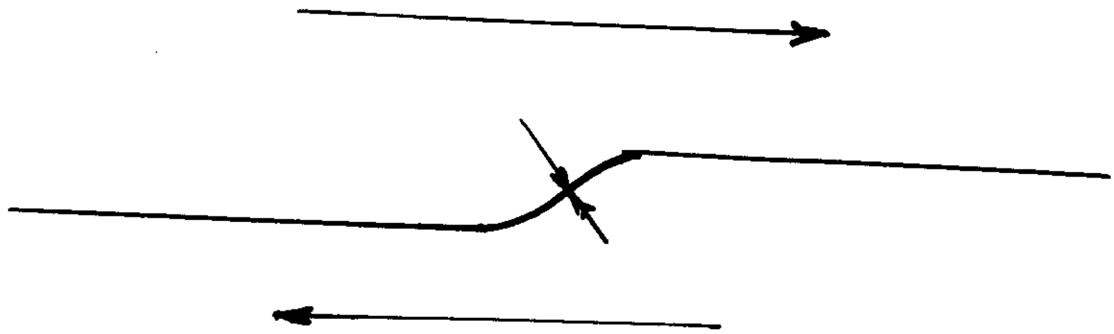

$$\sigma_t = \nu \sigma_n$$

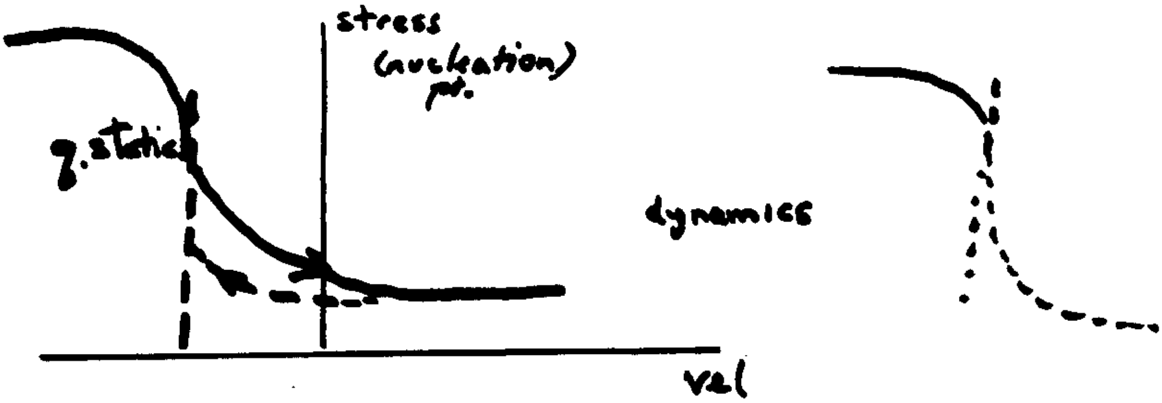


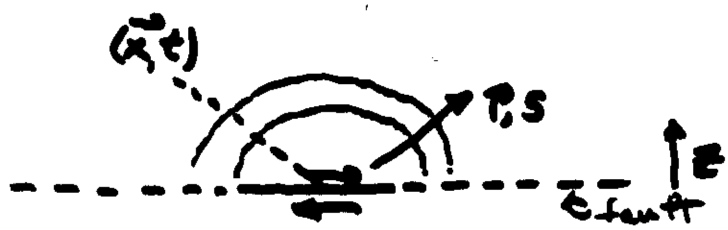


Elasticity

$$(\lambda+2\mu)\nabla\nabla\cdot\vec{U} - \mu\nabla\times\nabla\times\vec{U} - \rho\frac{\partial^2\vec{u}}{\partial t^2} = \vec{f}(x, y, 0, t)$$

displacement

$$\vec{u}(\vec{x}, t) = \int_{z=0} \overline{\overline{G}}(\vec{x}', t; \vec{x}, t)\,\overline{\tau}'\,dA'$$

no loading influence
(non linear!)

slip: $u(\vec{x}, t)_{z=0}$

Green's Functions: $$G = \frac{1}{\sqrt{(\vec{x}-\vec{x}')^2 - V_s^2(t-t')^2}}$$ 2-D antiplane

$$G = H\left[(x-x')^2 - c^2(t-t')^2\right]$$ 1-D

(no radiation) energy loss

2-D plane

3-D

Finite difference:

$$k\frac{\partial^2 u}{\partial x^2} \to k\left[u_{n-1} - 2u_n + u_{n+1}\right]$$

$$= k\left[u_{n+1} - u_n\right] - k\left[u_n - u_{n-1}\right]$$

n-1 n n+1

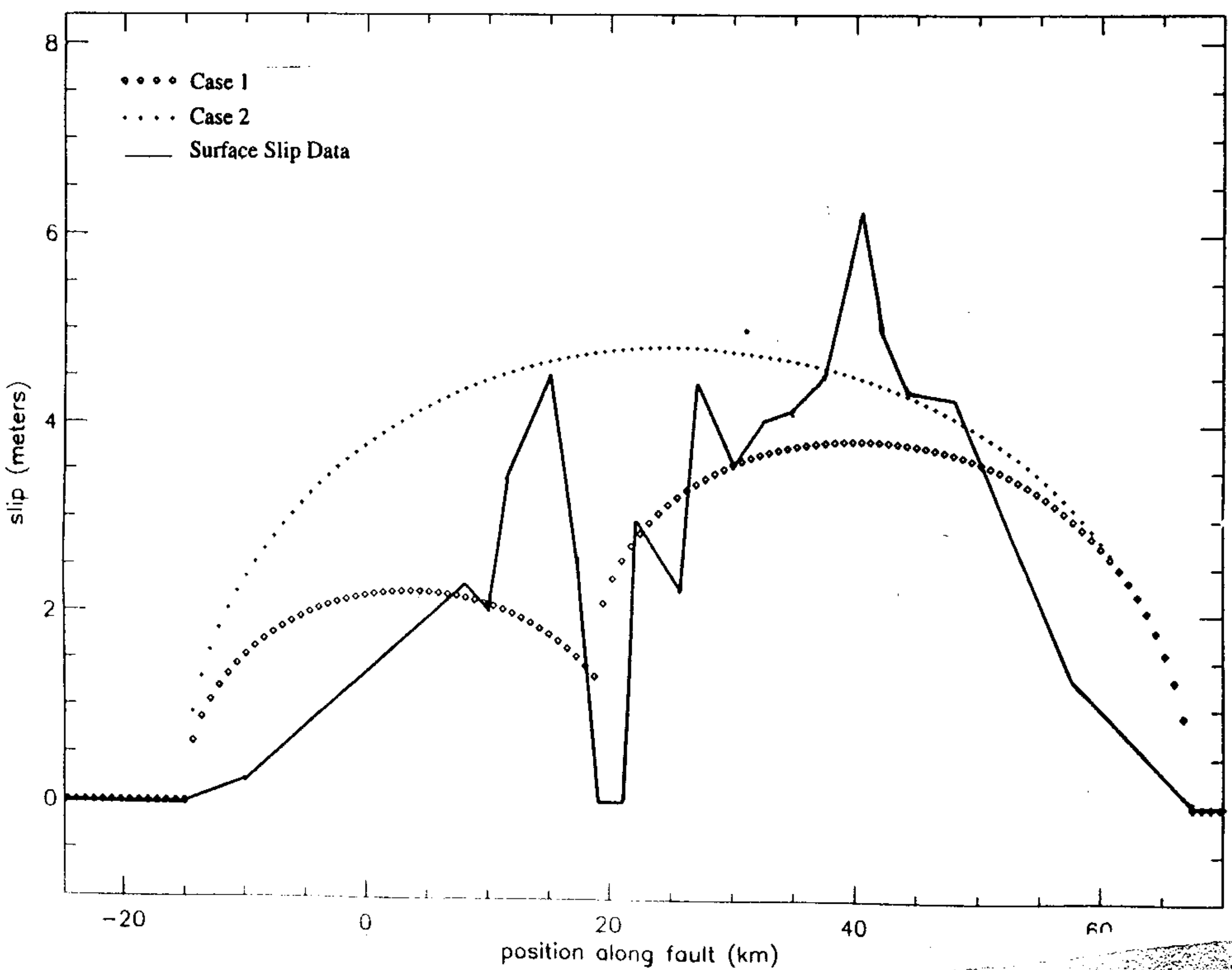

Case 1
Case 2
Surface Slip Data
slip (meters)
position along fault (km)
-20
0
20
40
60
0
2
4
6
8

15

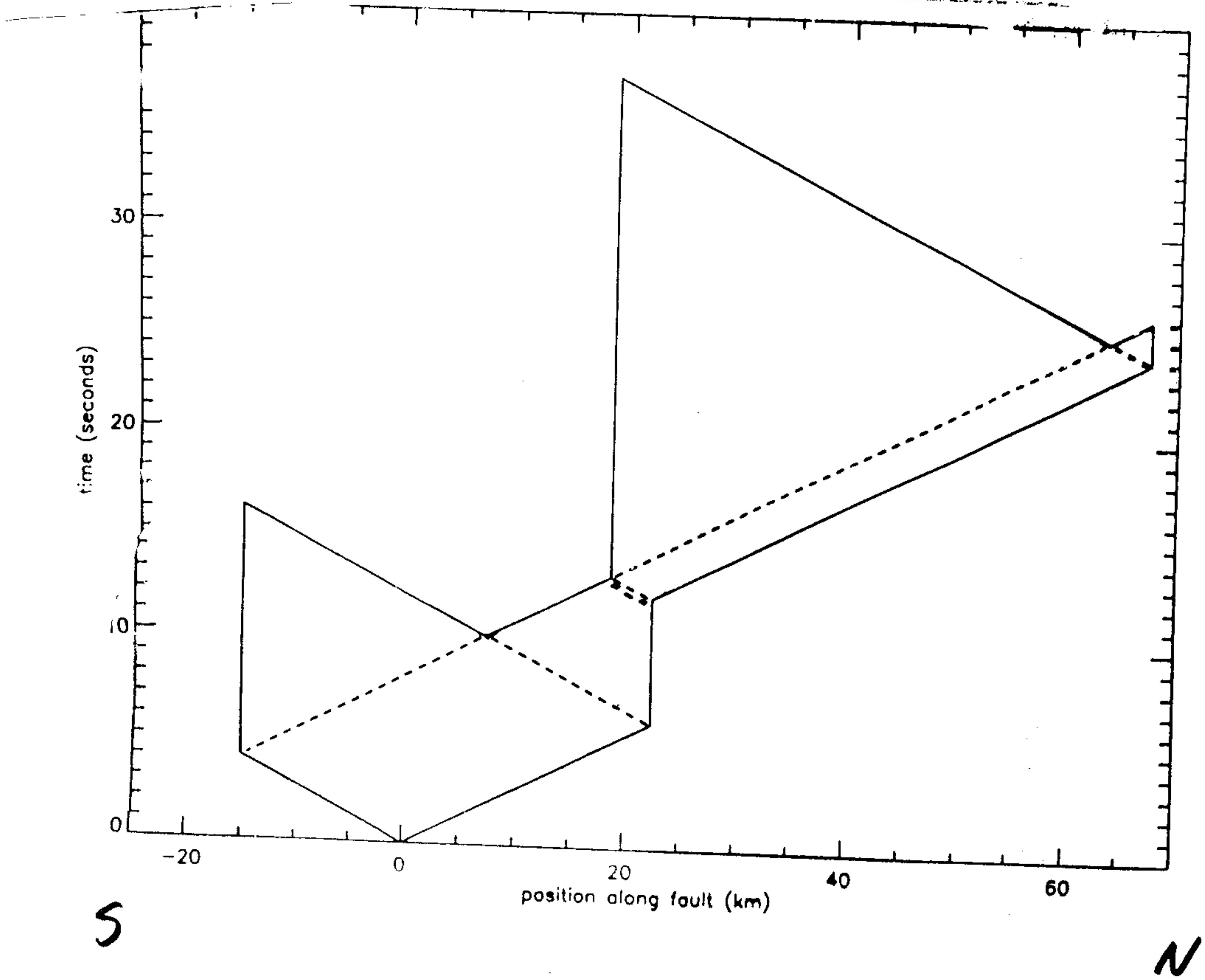

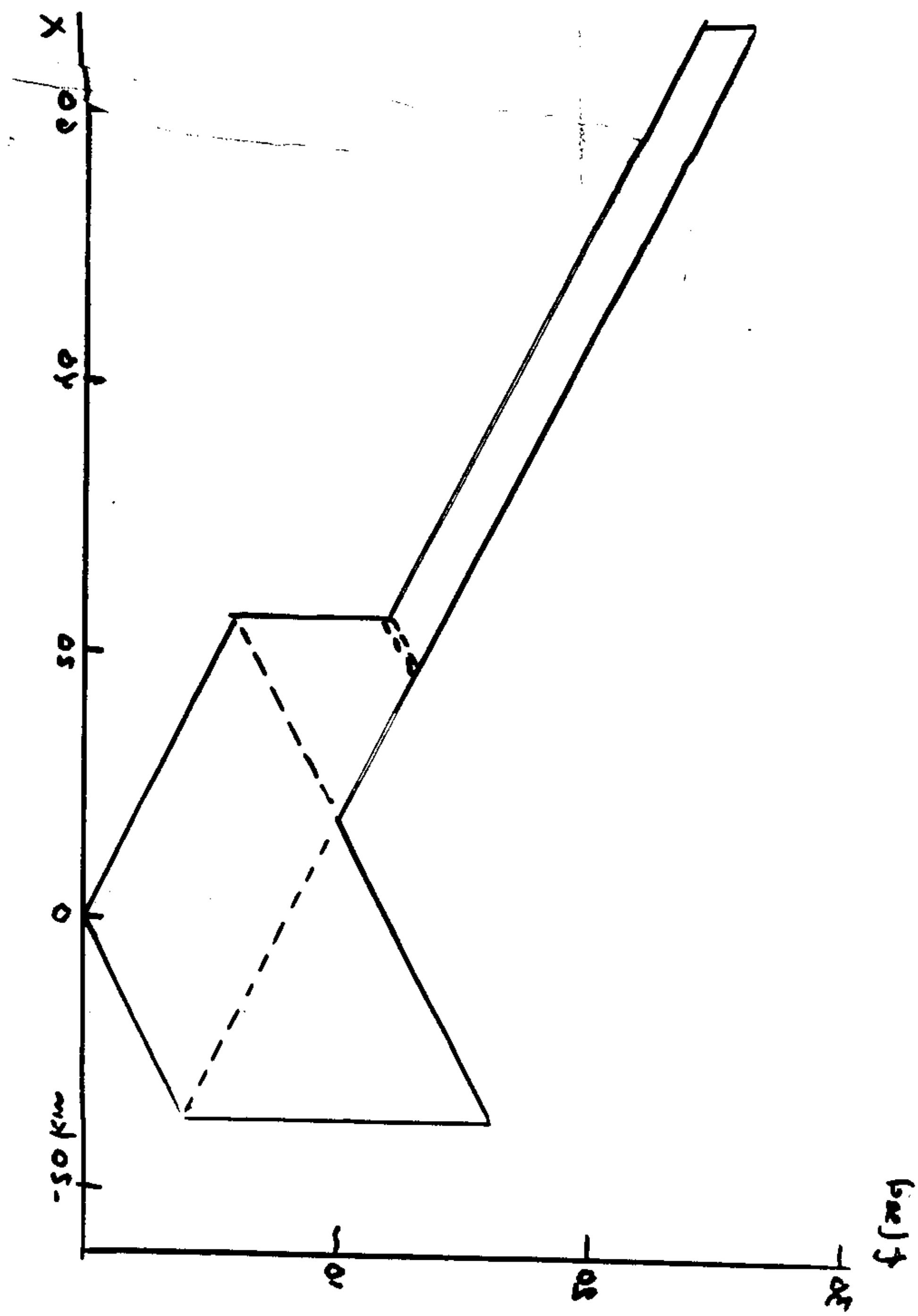
x
50
0
-50 km

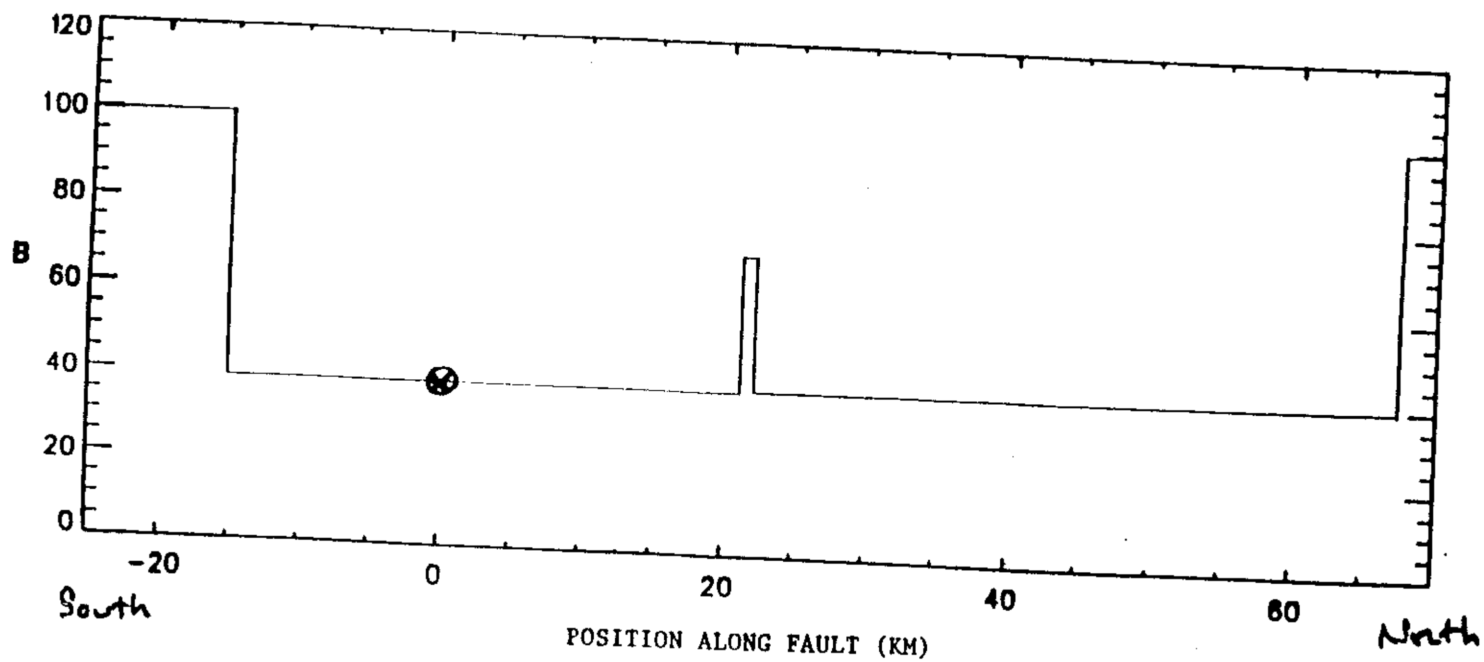
120
100
80
60
40
20
0
B
-20
0
20
40
60
South
North
POSITION ALONG FAULT (KM)

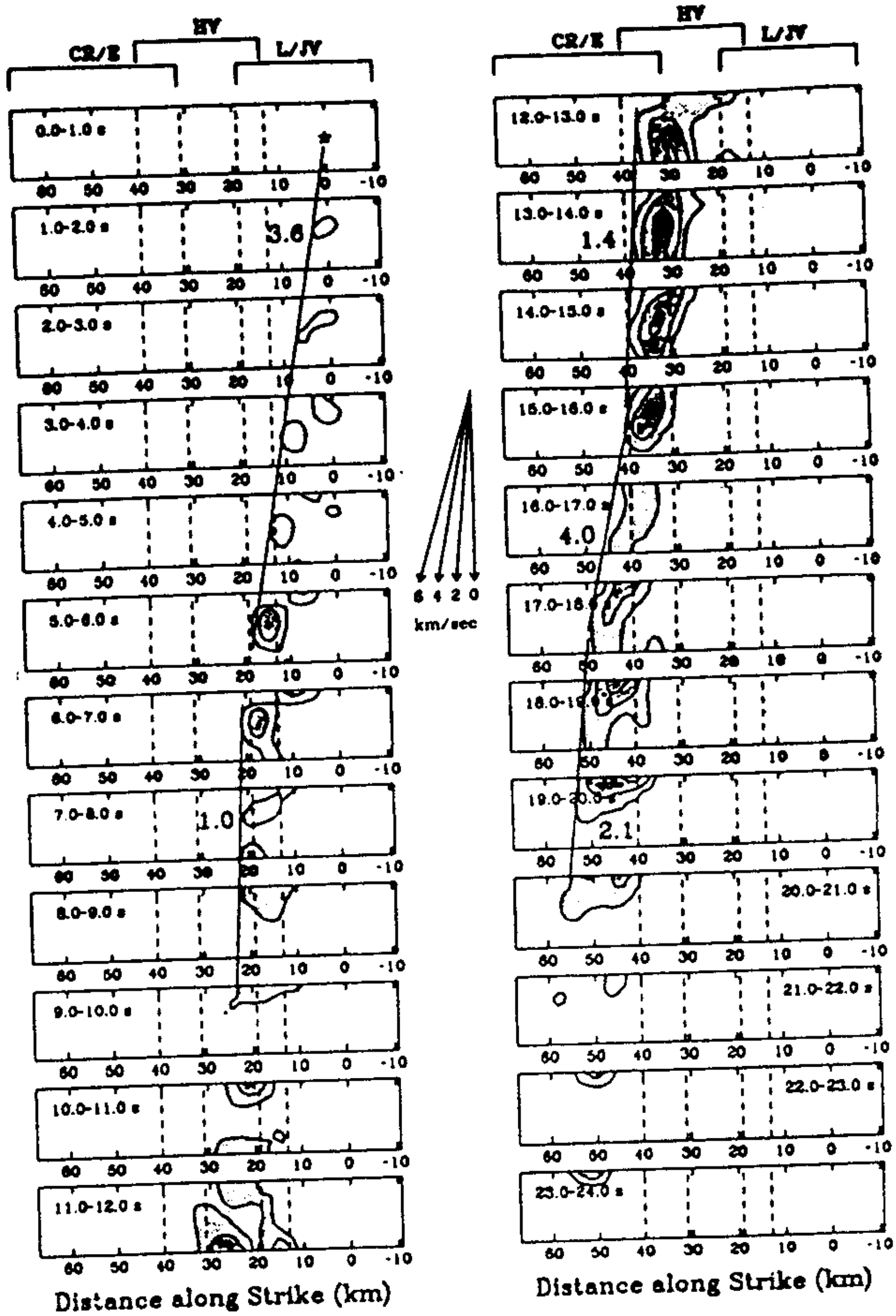
CR/E
HV
L/JV
0.0-1.0 s
1.0-2.0 s
2.0-3.0 s
3.0-4.0 s
4.0-5.0 s
5.0-6.0 s
6.0-7.0 s
7.0-8.0 s
8.0-9.0 s
9.0-10.0 s
10.0-11.0 s
11.0-12.0 s
12.0-13.0 s
13.0-14.0 s
14.0-15.0 s
15.0-16.0 s
16.0-17.0 s
17.0-18.0 s
18.0-19.0 s
19.0-20.0 s
20.0-21.0 s
21.0-22.0 s
22.0-23.0 s
23.0-24.0 s
3.6
1.0
1.4
4.0
2.1
6 4 2 0
km/sec
60 50 40 30 20 10 0 -10
Distance along Strike (km)
Distance along Strike (km)

Slip $\quad u \sim \frac{\sigma L}{\mu}$

For San Francisco 1906 $\quad u \sim 5\,\text{m}$

This gives $L \sim 15\,\text{km}$

But fracture length was 450-500 km!

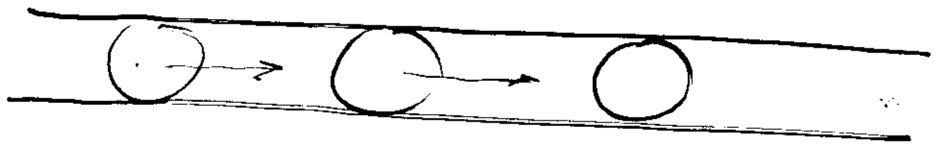

Standard Model

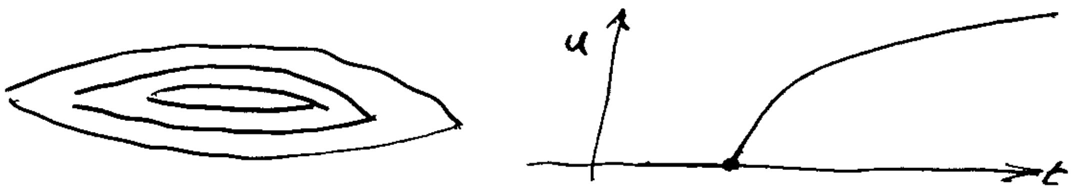


patch model